Journal of Rare Cardiovascular Diseases
ISSN: 2299-3711 (Print) | e-ISSN: 2300-5505 (Online)
www.jrcd.eu
RESEARCH ARTICLE

Hydroalcoholic Extract of Trapa natans L. Peel-Mediated Novel Zinc Oxide Nanoparticles: Development, Characterization, and Evaluation of Antioxidant, Anticancer, and Antibacterial Activities.

Swati Dubey[1,2], Yogendra Singh*[1], Shiv Kumar Yadav[2], Tarun Virmani[3]*, Ashwani Sharma[4], Mahima Chauhan[5]

[1]School of Pharmaceutical Sciences, MVN University, Palwal, Haryana, India
[2]BS Anangpuria College of Pharmacy, Faridabad, Haryana, India
[3]Amity Institute of Pharmacy, Amity University, Greater Noida, Uttar Pradesh, India
[4]Delhi Pharmaceutical Sciences and Research University, Delhi, India
[5]HIMT College of Pharmacy, Gautam Buddh Nagar, Greater Noida, Uttar Pradesh, India

*Corresponding Author
Prof (Dr.) Tarun Virmani

Article History
Received: 14.10.2025
Revised: 04.11.2025
Accepted: 25.11.2025
Published: 01.12.2025

Abstract: This research aimed to produce cost-effective, eco-friendly green metallic zinc oxide nanoparticles (ZnO NPs) by using 50% hydroalcoholic extract of Trapa natans L. peel (TPHE) and evaluate their antibacterial, antioxidant, and anticancer bioactivities for the first time. The hydroalcoholic extract of T. natans peel is rich in several flavonoids and phenolic constituents that serve as stabilizing agents, reducing agents, and capping agents in developing NPs. The Ultraviolet-visible spectroscopy (UV-Vis) shows maximum absorbance at 368 nm, confirming NPs synthesis. The mean diameter of NPs was 94.26 nm with -19.9 mV zeta potential. Furthermore, transmission/scanning electron microscopy (T/SEM) demonstrated a spherical morphology and nanometer-sized particles. Additionally, Energy Dispersive X-ray Spectroscopy (EDS) confirmed Zn and Oxygen (O) presence. After characterization, bioactivities of developed NPs and peel extract were evaluated, where ascorbic acid, doxorubicin, and ciprofloxacin were taken as standards. Antioxidant activity was evaluated by 2,2'-azino-bis (3-ethylbenzothiazoline-6-sulfonic acid (ABTS), diphenyl-picrylhydrazyl (DPPH), and ferric-reducing antioxidant power (FRAP) techniques. Moreover, ZnONPs demonstrated potential anticancer activity towards SK-OV3 (IC50 value- 20.50 ± 0.0807 µg/ml) and A549 (22.85 ± 0.07 µg/ml) malignant cells, and were noncytotoxic towards VERO cell lines. Additionally, ZnO NPs demonstrated excellent antibacterial action towards Enterococcus faecalis (E. faecalis), Escherichia coli (E. coli), Bacillus subtilis (B. subtilis), and Pseudomonas aeruginosa (P. aeruginosa) in comparison to TPHE. Conclusively, this research focused on producing novel ZnO NPs by utilizing 50% hydroalcoholic extract of T. natans peel, exhibiting potential antioxidant, anticancer, and antibacterial activities.

Keywords: Green synthesis; Trapa natans peel; Hydroalcoholic extract; Zinc oxide NPs; Antioxidant; Antibacterial; and Cytotoxic/Anticancer activity..

Graphical Abstract

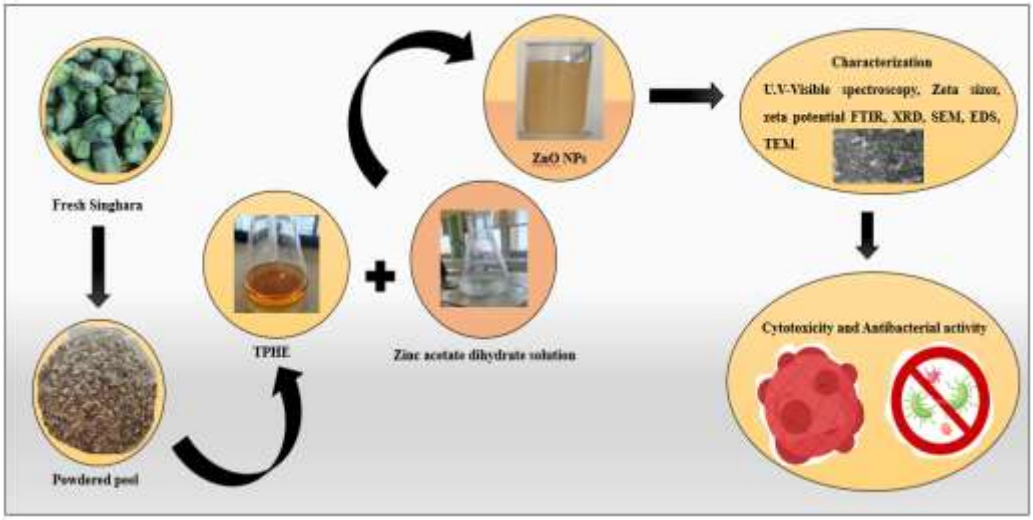

Highlights of Paper:

- This study synthesized environment benign ZnO NPs utilizing *T. natans* L. peel hydroalcoholic extract (TPHE) and evaluated their biological activities.
- The hydroalcoholic extract (50%) of *T. natans* peel, rich in poly phenolic constituents and flavonoids, acted as reducing, capping, stabilizing agents during synthesis.
- UV-Vis spectroscopy confirmed ZnO NPs formation (λmax = 368 nm), showing mean size 94.26 nm and -19.9 mV of zeta potential.
- Characterization via SEM, TEM, and EDS analysis confirmed the spherical shape, nanometer size, and elemental composition (Zn and O).
- ZnO NPs demonstrated strong antioxidant activity (DPPH, ABTS, FRAP assays) and potent anticancer effects on SK-OV3 and A549 cell lines, with no cytotoxicity towards VERO cells.
- Additionally, in comparison to TPHE, NPs demonstrated superior antibacterial action towards tested microorganisms, including *B. subtilis, E. coli, E. faecalis, and P. aeruginosa*.

INTRODUCTION

The persistent growth in cancer cases has created an alarming situation throughout the globe. After cardiovascular diseases, it is one of the prominent reasons for death worldwide[1]. Various treatment modalities, including immunotherapy, radiotherapy, aromatherapy, surgery, and chemotherapies, are available to treat cancer; nevertheless, chemotherapeutic drugs are highly demanding and a commonly utilized therapy.[2]. Strong medications are used in chemotherapy to target rapidly dividing cells. These medications face several challenges, such as numerous side effects, drug resistance, patient discomfort, insensitivity to cancer drugs [3]. Consequently, there is a growing need for more targeted and less toxic therapies, such as those offered by advancements in nanotechnology and nanomedicine, which promise to improve efficacy while minimizing harmful side effects[4]. Similarly, the increase in microbial infections like COVID-19 has led to intensified use of antimicrobial drugs (antibiotics), which evolved antimicrobial resistance worldwide. In 2019, approximately 5 million fatalities occurred due to antimicrobial resistance, and if ignored they may rise to 50 million. As a result, it is crucial to find novel substances with antimicrobial and anticancer properties[5].

To deal with the issues related to cancer and antimicrobial resistance, tiny NPs have drawn attention due to their large surface area, as well as their magnetic, optical, mechanical, and chemical properties, along with high stability, improved safety, and low cost[6]. Several metals (silver, zinc, iron, gold, copper) and metal oxide (MO) (zinc oxide, iron oxide, cobalt oxide, copper oxide, selenium oxide, titanium dioxide) NPs can be manufactured effectively by a variety of physicochemical techniques including laser irradiation, laser ablation, thermal decomposition, chemical reduction, lithography, and electrochemical reduction[7,8]. However, most of these traditional synthetic methods are extremely expensive and require harmful reducing agents, which show adverse effects on the environment and living beings[9] Hence, to overcome the limitations of physiochemical methods, this research focused on biological or green synthesis, which offers several significant advantages, including environmental friendliness, low cost, low toxicity, and quick production. Green synthesis involves plant extracts that contain various phytoconstituents, including phenolic constituents, flavonoids, alkaloids, tannins, glycosides, and saponins, that work as capping, stabilizing, and reducing agents in green MONPs synthesis [10].

ZnO NPs have become the most popular among various plant-mediated NPs in the last 20 years because of their wonderful biological, chemical, and physical properties[11]. They have superior biocompatibility with human cells over zinc metal and can be readily absorbed by biological tissues due to low toxicity and excellent chemical stability. It has excellent semiconductor properties, having a wide band gap with 60 meV (high excitation) binding energy. ZnO is a reliable substance permitted by the Food and Drug Administration (US) [12]. Zinc is considered as safest element for protecting human health, due to its superior antibacterial properties. Consequently, ZnO nanoparticles (NPs) are utilized in various industries, including healthcare, cosmetics, food, and agriculture. Accordingly, many researchers worked on various plant species to develop ZnO NPs and reported their potent antibacterial, antioxidant, and anticancer activities[13–15]. A few examples are *Punica granatum* fruit peel extract [16], *Phlomis* leaf extract [17], *Actinidia deliciosa* fruit peel extract [18], *Pluchea indica* leaf extract [19], *Solanum lycopersicum* fruit juice [20], *Olea europeae* fruit extract [21], *Allium cepa L.* peel extract [22], banana peel and date seed extract [23]. Based on these findings an adequate zinc precursor was extracted which further combined with 50% hydroalcoholic extracts of *T. natans* peel. Overall, novel ZnO NPs were synthesized in this research for the first time by utilizing hydroalcoholic peel extract of *T, natans* L. via an advanced eco-friendly and cost-effective approach that imparts synergistic biological activity of the peel and a metal precursor.

T. natans L. (Caltrops/ Singhara nut) grows in water, termed as a watery plant, belongs to the "*Trapaceae"* family, which has several therapeutic benefits. In ancient times, the fruit was used to make salves for treating rheumatism, wounds, and sunburn. The juice

extracted from the stem has also been traditionally utilized for curing eye disorders. Singhara fruit is popular for its superior antibacterial, immunomodulatory, antidiabetic, anti-inflammatory, antiulcerogenic, and weight management properties. In addition, it also exhibited potential antioxidant and anticancer activity towards free radicals, as peel contains bioactive constituents like phenolics, flavonoids, or other phytochemicals, including carbohydrates, glycosides, proteins, and vitamins. The polyphenolic constituents are natural antioxidants that scavenge free radicals by donating hydrogen atoms or an electron and reduce the harmful effects of free radicals, leading to a reduction in oxidative stress and prevention of biological components such as proteins, lipids, carbohydrates, and DNA [24,25]. Biological activities of *T. natans* "fruit" have been extensively researched[26]. However, only a few studies have examined the biological activities of *T. natans* "peel", which is typically considered a waste material and often discarded after consuming edible parts (fruit). Moreover, the phenolic content of *T. natans* peels is significantly higher than its fruits. Hence, based on these findings, this research focused on an eco-friendly, cost-effective process to synthesizing novel ZnO NPs by utilizing hydroalcoholic extract (50%) of *T. natans* L peel. Additionally, the data gives detailed information regarding the physiochemical characterizations of novel ZnO NPs and evaluates their antioxidant effect, anticancer potential, and ability to inhibit pathogenic bacteria (antibacterial potency).

MATERIALS AND METHODS

2.1. Sample Collection Method

T. natans fruits were brought from a local fruit vendor in the Faridabad district of India. Further, they were washed properly with water and wiped by using cotton cloth. After that peel was removed from the fruits and dried (peel) under shade for approximately two to three months. Dr. Sunita Garg authenticated the dried sample under authentication details NISCPR/RHMD/Consult/2022/4379-80-2-, at Raw Materials Herbarium and Museum Delhi (RHMD).

2.2 Chemicals and Reagents

Reagents used in this research were linked from various suppliers such as Ascorbic acid obtained from (SD Fine, India - Cat no. F13A/0413/1106/62), Methanol (Cat no.- 10930lC250), and Dimethyl Sulfoxide (DMSO, Cat no.28580), DPPH - (Cat no.- SR-29128), ABTS (SRL-Chem-Cat no.-28042), Mueller-Hilton Agar (MHA, Cat no.-24756), sodium phosphate buffer (Rankem, Cat no.- S0240), 0.1% ferric chloride (Fischer scientific- Cat no. 23585),1% potassium ferricyanide ($K_3Fe(CN)_6$- Cat no.- 15766),10% trichloroacetic acid (Cat no.-92390) and Ciprofloxacin (78079), was procured from SRL Chem India, Doxorubicin (Celon Labs- DR12403BC), Microbial Cultures were obtained from Gene Bank, and Microbial Type Culture Collection (MTCC), Chandigarh. Cell lines for each specific cancer were procured via the National Centre for Cell Science (NCCS), Pune, India.

2.3. Method to prepare hydroalcoholic extract (50%) of *T. natans* L. peel

To prepare a 50% hydroalcoholic extract of *T. natans* peel, initially, the peel was dried well and crushed into a coarse powder. Later, it was mixed with the solvent in a 1:10 ratio, as shown in **Figure (Fig.) 1**. Accordingly, 10 g of *T. natans* peel powder was added to 100 mL of prepared solvent (containing 50 mL of ethanol and 50 mL of distilled water). Further, this solvent containing peel powder was kept on a magnetic stirrer for 24 hours at room temperature to facilitate extraction. Afterward, it was filtered through a filter paper (Whatman- 0.45 µm) and kept in the refrigerator at 4°C for further synthesis and characterization purposes. The hydroalcoholic extract was prepared using the method mentioned by Hashem et al. and Al-Khaial et al.[27,28] with a few modifications.

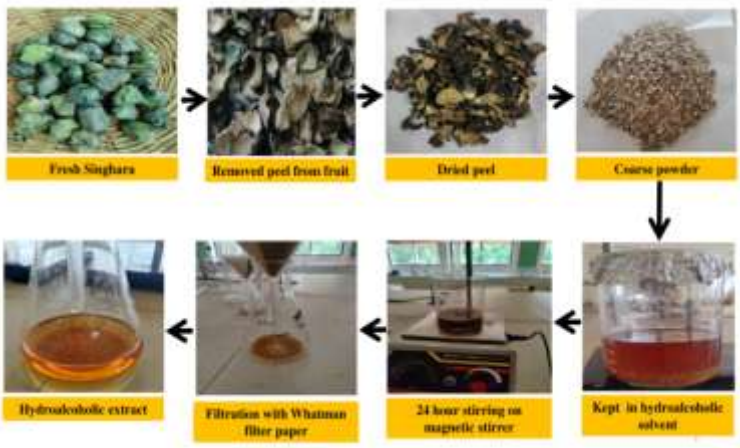

Fig. 1. Flow chart representing the preparation process of 50% hydroalcoholic extract from *T. natans* L. peel.

2.4. Qualitative analysis of phytochemical

The **Qualitative** screening of phytochemicals was performed in the laboratory to identify the presence of active phytoconstituents in prepared TPHE such as phenolic compounds, tannins, flavonoids, glycosides, alkaloids, proteins, carbohydrates, and lipids. These phytoconstituents are known for their antimicrobial, anticancer, and antioxidant action. They also behave as stabilizers or reducing agents, showing capping property in the developing ZnO NPs [29][30]. All tests were performed in triplicates according to the standard procedures, and two or more identification tests were examined for each category.

2.5. Quantitative analysis by LC-MS/MS

The phenolic compounds and flavonoids have a higher capacity to reduce the metal ions into the NPs, so their presence was characterized by the LC 1200 Series, 6470 MS Agilent (USA). The Mass Hunter software performed data acquisition and processing. Using the Soxhlet apparatus, samples (freeze-dried) were extracted for 24 hours in 10 mL of methanol**,** and then it was dried at 40 °C in a rotary evaporator. Finally, the volume was made up with 1 ml of solvent and run onto a column C18 (2.1 × 2.7, 100mm (poroshell) with 55 °C column temperature and 5 µl injection volume. The mobile phase was prepared using two eluents, one is made up of 0.1% formic acid in water (eluent A) and the other is methanol (eluent B). The mobile phase was added in varying concentrations over time with a flow rate of 1 ml/min. The concentration gradient of eluent A was like this- A 95% (0 min), 95% (0.5 min), 60% (10 min), 40% (12 min), 5% (15 min), 5% (16 min), 90% (18 min), 95% (20 min). After exiting the column, the components are injected into a nebulizer, which disperses the liquid into a fine mist; this is termed an electrospray ionization technique. Mass analysis was done using the electrospray ionization technique, where high-purity nitrogen was applied[31]. The conditions for mass spectrometry were: 2000 V (voltage) of capillary; 500V of nozzle; 6 l/min flow of drying gas; 12 ml/min of sheath gas; 300°C of sheath gas temperature; 225°C of gas temperature; and nebulizer pressure of 50 psi. With the help of retention time, mass spectrometry data, and UV spectra comparison with the reference compounds, which are documented in the literature.

2.6. Preparation of metal precursor solution

Different concentrations (0.001M, 0.01M, 0.1M) of Zinc acetate dihydrate were used to prepare metal salt solutions. Accordingly, the accurate amount (0.02195 gram (gm), 0.2195 gm, 2.195 gm of zinc acetate dihydrate was weighed and mixed in 100 mL of distilled water, and dissolved completely. Salt solutions were carefully stored in volumetric flasks at room temperature with proper covering.

2.7. Development of green ZnO NPs

To develop green ZnO NPs, 0.1 M (50 ml) of zinc acetate dihydrate aqueous solution was added to 100 mL of 50% TPHE (50 mg/mL). This mixture was kept on a magnetic stirrer at room temperature for 1 hour at 250 revolutions per minute (rpm). The pH was maintained at 7.0 using a 1M sodium hydroxide (NaOH) solution. Afterward, it was incubated for another 1 hour at room temperature. Further, centrifugation was performed at 6000 rpm for approximately 2 minutes, and a clear supernatant was obtained along with settled pellets. Accordingly, supernatant was discarded, and pellets were collected using a narrow-tip spatula. The pallets were then washed twice with ethanol and then with distilled water (six times) to discard any remaining impurities or zinc acetate dihydrate. Finally, the NPs were dried at 40ºC for 2 hours and stored well at 4°C in a refrigerator for further characterization and bio-activity determination. **Fig. 2 demonstrates** a step-by-step procedure for developing ZnO NPs.

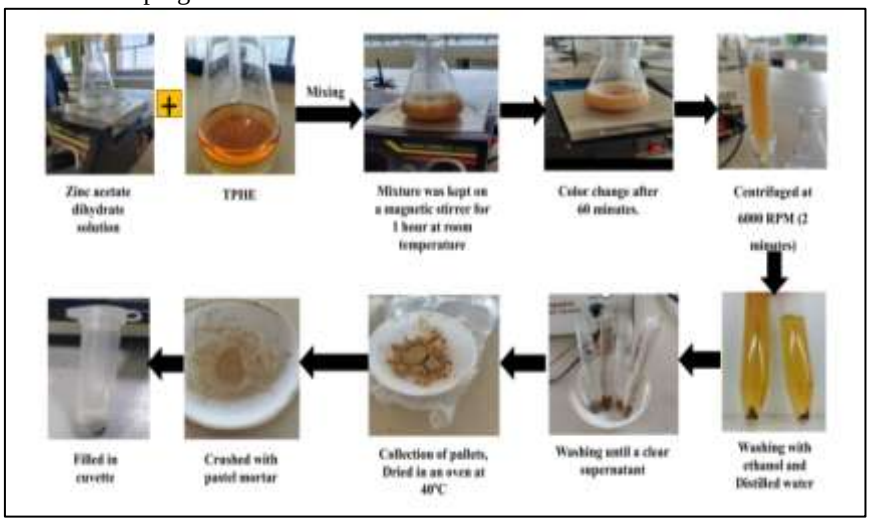

Fig. 2. Diagrammatic representation of the development process for ZnO NPs by utilizing 0.1 M zinc acetate dihydrate as a metal precursor and TPHE as an extract.

Journal of Rare Cardiovascular Diseases
ISSN: 2299-3711 (Print) | e-ISSN: 2300-5505 (Online)
www.jrcd.eu

RESEARCH ARTICLE

2.8. Optimization of green ZnO NPs

The developed ZnO NPs were optimized by an Ultraviolet-Visible (UV-Vis) Spectrophotometer. For this, a dried sample of ZnO NPs was dispersed in a 50% hydroalcoholic solvent and kept in a quartz cuvette for spectral analysis. To investigate the concentration effect of metal precursor solution on NPs synthesis, different sets of zinc acetate di-hydrate salt solution (0.001M, 0.01M, 0.1M, 0.2 M) were mixed with peel extract solution (50 mg/mL) in 1 to 1 ratio (1:1). Further mixture was kept in normal room temperature and stirred with a magnetic stirrer at 250 rpm until the visible colour changes. To check the effects of the peel extract concentration on the development of NPs, 10 mL of Zinc acetate dihydrate (0.1 M) solution was combined with five different sets (volumes) of peel extract, starting from 5 mL up to 25 mL with a difference of 5 mL in each set. Further time optimization can be achieved by making four different sets. Each set contained a fixed ratio (1:2) of metal salt precursor (0.1 M) and peel extract (50 mg/mL), and was kept at 250 rpm on a magnetic stirrer for different time intervals starting from ½ an hour up to 2 hours, with 30 30-minute gap in each set. Confirmatory analysis of the synthesis for each sample was performed using a UV-Vis spectrophotometer.

2.9. Characterization Parameters

2.9.1. UV-Vis Spectroscopy

Double-beam UV-Vis Spectrophotometer (Systronics - 2201, India) was utilized initially to detect the successful production of green ZnO NPs. For this, synthesized NPs were dispersed in a suitable solvent and kept in the quartz cuvette. Spectra were observed in the 200 nm to 500 nm range at 1 nm resolution. Before measuring the samples, it's important to auto-zero the instrument using a sample that does not contain any known metal salts[32].

2.9.2. Size, Surface Charge, Morphology, and Element Composition Determination

The physical and chemical properties of the hydroalcoholic extract of *T. natans* peel-mediated ZnO NPs, were determined using six different techniques including Zeta sizer, Zeta potential, EDS, SEM, TEM, and XRD which gave complete information regarding size, shape, morphology, surface charge, crystallinity, and elemental details of NPs [33]. These methods evaluated the size distribution and NPs size in colloidal solution.

2.9.3. X-ray diffraction examination

XRD is an effective way for characterizing the crystallinity and polycrystallinity of nanomaterials. Bruker D8 Advance, XR-Dynamic 500 was used to examine information about the phases, structure, texture, and other constraints, including crystal defects, average grain size, and crystallinity. The instrument consists of several key components: an X-ray source, sample holder, mount, tube housing, goniometer, slit systems, and detector with optics. It is equipped with DIFFRAC (TOPAS software, EVA evaluation software) for analysing diffractograms, as well as the ICDD PDF-4 Axiom 2020 database[33]. Additionally, crystallite size was measured using the Debye-Scherrer equation, after scanning in a 2θ (20–80º) range. The equation as follows:

$$\mathbf{D = K \lambda / \beta \cos \theta}$$

where D = particle diameter/crystallite size in nm
K= 0.9 (Scherrer constant)
λ= 1.5406 Å (wavelength of X-ray radiation)
β= full width at half maximum in Radians
θ= Bragg angle in radians (Peak position half diffraction)

2.9.4. Morphological characterization via TEM, SEM, and EDS

The size and morphology of the developed NPs were determined by electron microscopic techniques, and elemental composition was analysed using the EDS method. In the EDS technique, the INCA x-act EV Dry Detector from OXFORD Instruments of the UK is typically coupled with SEM (JSM 6490), where the X-ray detector is placed next to the sample to analyze the emitted X-rays. In the SEM unit, the preparation of samples for performing SEM has been supported by two units, such as the Critical Point Dryer of UK (Emitech K 850 of Quorum Technology), and the Sputter Coater of JEOL, Japan (JFC 1600, Auto Fine Coater). The SEM images were scanned using Image J software to measure the average size of ZnONPs. Moreover, TEM was also performed to monitor the accurate shape and size of the developed NPs. To ensure effective dispersion, the produced NPs were sonicated with Milli-Q water. A few drops were put on the TEM carbon grid, let them dry, and examined further[34].

2.9.5. FTIR Study

The investigation of functional groups in synthesized ZnO NPs was detected by FTIR spectroscopy, where the involvement of 50% hydroalcoholic extract can be detected easily [35]. In this method, solid powder samples were first dried in an oven, then crushed finely, and mixed in a 1:10 weight ratio of potassium bromide (KBr). Afterwards, this mixture was pressed at 15000 psi to prepare discs. These discs were then scanned at a wavelength ranging from 400-4000 cm^{-1}, using the FT-IR Nicolet, USA6700 instrument[36].

2.10. Antioxidant potential

The antioxidant potential of 50 % TPHE and synthesized ZnO NPs was examined via three antioxidant assays, including DPPH, ABTS, and FRAP assays. Different concentrations were prepared for both TPHE and developed NPs (0.78, 1.56, 3.125, 6.25, 12.5, 25, and 50 µg/ml), whereas ascorbic acid (standard

drug) was taken for comparative analysis. GraphPad Prism 6 software was utilized to measure the IC_{50} of all samples, and a graph was created between the X-axis and Y-axis, representing sample concentration v/s percentage inhibition compared with the control.

2.10.1. DPPH Assay

In the DPPH radical assay, 5µl of different stocks of test compounds (TPHE, ZnO NPs, and ascorbic acid) was placed in a 96-well plate along with 0.1 mM DPPH (1 mL) solution. All reactions were placed in quadruplicate form, and duplicates of the blanks. Blanks were prepared using 5µl of test compounds with a concentration range (0.78, 1.56, 3.125, 6.25, 12.5, 25, 50 µg/ml, where 0 µg/ml was taken for control), along with 0.2 mL of Methanol. The well plate with no treatment was termed as the control, and the wells that lacked the DPPH reagent were termed as blanks. Further incubate the plates in a dark place for 30 minutes. Afterwards, the sample decolorization was read using an iMark, Bio-Rad microplate reader at 517 nm[37]. The formula used to determine percent inhibition for DPPH activity is:

$\%RSA = ((Abs_{Control} - Abs_{Sample})/Abs_{Control}) \times 100$

where, RSA = Radical Scavenging Activity

$Abs_{Control}$ = Control absorbance

Abs_{Sample} = Sample absorbance

2.10.2. ABTS) Assay

In the ABTS assay, ABTS radicals were prepared initially by adding 2.45 mM of APS and 7 mM of ABTS. This solution was further diluted up to 100X to make ABTS reagent. After this, 200µl of ABTS reagent was added with 10µl of various concentrations of TPHE, synthesized NPs, and ascorbic acid in 96-well plates, and incubated for 10 minutes in the dark at room temperature. After successful incubation, decolorization was measured at 750 nm. The wells without treatment were considered as controls[38]. The formula used to measure the percent radical scavenging activity for the ABTS assay is:

$\%\ RSA = ((Abs_{Control} - Abs_{Sample})/Abs_{Control}) \times 100$

2.10.3. FRAP Assay

To estimate FRAP activity**,** 10µl of various concentrations of TPHE, synthesized NPs, and standard ascorbic acid was mixed with 0.2 M sodium phosphate buffer (0.04 mL with a pH of 6.6) along with 1 % $K_3Fe(CN)_6$ (0.05 mL) solution. After proper mixing, it was incubated for 20 minutes in a dark place at 50°C. After incubation, 0.5 ml of trichloroacetic acid (10%), 50µl of ferric chloride (0.1%), and 50µl of deionized water were added one by one. Absorbance was measured using a microplate reader at 700 nm against a blank[39]. The following formula calculates the scavenging activity is:

$\%\ FRAP = (A_{Sample} - A_{Control}/A_{Control}) \times 100$

2.11. Evaluation of Cytotoxic Potential

To investigate the cytotoxic potential of developed ZnO NPs and TPHE against ovarian adenocarcinoma (SK-OV3), lung adenocarcinoma (A549), and Kidney normal cell line (Vero), an MTT assay was performed. All cell lines were acquired from NCCS Pune, and 10000 cells/well were grown in 96-well plates and incubated (Air-Jacketed CO_2 incubator, Heal Force-HF90) in DMEM medium (Dulbecco's Modified Eagle Medium-AT149-1L- HIMEDIA) supplemented with FBS 10% (Fetal Bovine Serum - HIMEDIA-RM 10432) and antibiotic 1% solution (Penicillin-Streptomycin-Sigma-Aldrich P0781) for 24 h, at 37°C with 5% carbon dioxide. After 24 hours, all the cells were treated with TPHE, ZnO NPs, and Doxorubicin (standard drug) in several concentrations, such as 100, 50, 25, 12.5, 6.25, 3.125, 1.5 µg/mL, and 0 (for control wells). Afterward, the MTT medium was discarded, and 100 µL of DMSO reagent was added to each well to dissolve MTT formazan crystals. The absorbance was measured at 540 nm using an ELISA plate reader. The non-treated cells showed 100% survival rate, considered as controls, and cells that lacked the MTT reagent were taken as blanks, which helps in calibration (zero absorbance). Images were captured under an inverted microscope (Olympus ek2) using a Camera (AmScope digital camera 10 MP Aptima CMOS). The cell viability percentage (%) was determined using the formula:

Cell Viability % = (Abs_{test} / $Abs_{control}$) *100

(Abs_{test} = Absorbance of the test sample, $Abs_{control}$ =Absorbance of control)

2.12. Antibacterial activity

The antibacterial action was assessed by the disk diffusion (Kirby-Bauer) method [41], for all the tested strains (gram-positive and negative), including *Enterococcus faecalis* (*E. faecalis):* MTCC 439, *Bacillus subtilis* (*B. subtilis):* MTCC 1133, *Escherichia coli (E. coli):* MTCC- 452, and *Pseudomonas aeruginosa* (*P. aeruginosa)*: MTCC- 3541. The MHA plates were sterilized and allowed to solidify. Once solidified, bacterial cultures (100 µl) were inoculated with a sterile glass rod. The Inoculum was prepared by adjusting the cell density approx 1.5 X 10^8 CFU/mL (0.5 McFarland Unit) from Mueller-Hinton Broth, followed by placing the discs containing 10µl of synthesized ZnO NPs and TPHE in different strengths: 6.25, 12.5, 25, 50, and 100 µg/mL. As vehicle control, DMSO was placed into each plate. Furthermore, 10µg of Ciprofloxacin (standard) was considered as a positive control. All tested plates were kept in an incubator (Basil Scientific Corp. India- Incubator) for 24 24-hour intervals at 37 °C. The clear zones appeared after the incubation, which were measured in millimeters (mm) using a transparent scale[42]. Triplication was done for all samples, inhibition zones was presented as Mean ± SD[43].

2.13 Statistical analysis

The particle size of developed NPs was determined by XRD and SEM, by utilizing Origin and Image J software. All data were represented as Mean ± SD

(Standard Deviation) and calculated by GraphPad Prism 6 software. The statistical significance of values was estimated by one-way ANOVA and Tukey's post hoc test. The level of significance for all data is $P< 0.05$.

RESULTS AND DISCUSSIONS:

3.1. Qualitative analysis of Phytochemicals

Qualitative phytochemical screening revealed positive results for various bioactive constituents, including alkaloids, flavonoids, phenolic compounds, tannins, and glycosides. These bioactive compounds reduce or stabilize the synthesized ZnO NPs and act significantly in the entire process. **Table 1** represents detailed findings of the preliminary phytochemical analysis. Data indicated a significant presence of phenolics, carbohydrates, flavonoids, and other phytochemicals in the 50 % TPHE. The high levels of flavonoids and phenolic constituents suggest their effectiveness in the green synthesis of NPs, as they are more likely to reduce metal precursors into MONPs. The high presence of carbohydrates can act as a stabilizing agent for metal oxide NPs, binding to their surface, which helps prevent aggregation and enhances stability[44].

Table 1. **Qualitative phytochemical screening** of TPHE

S. No	Type of Phytochemical	Test	Colour Indication	Presence in TPHE
1.	Alkaloids	Dragendorff's	Orange-red ppt	-
		Hager's	Yellow ppt	-
		Mayer's	Yellow/White ppt	-
		Wagner's	Reddish brown ppt	-
2.	Carbohydrates	Benedict's	Orange/blue/green/red ppt	+++
		Molish	The purple ring at the junction	+++
3.	Phenolic compounds and Tannins	Ferric chloride	Red/green/ blue/purple color	+++
		Lead acetate	White ppt	+++
4.	Protein and Amino acids	Ninhydrin	Deep blue appearance	++
		Biuret	Purple colour	++
5.	Flavonoids	Sinodha	Orange colour	+++
		Alkaline reagent	Deep yellow tint	+++
6.	Steroid	Salkowski	Chloroform layer is red, and yellowish-green fluorescence shown by sulphuric acid layer.	-
7.	Saponins	Foam test	Appearance of foam	-
8.	Glycosides	Keller-Kilian	Ring created by the brown colour at the interface	++
		Borntrager's	Pink to red color	++
9.	Fixed oils and fats	Spot test	A translucent spot appeared	-ve
		Sudan III test	Red-stain oil layer	-ve

Absence (-ve), low presence (+), moderate presence (++), high presence (+++).

3.2. Quantitative analysis by LC-MS/MS

Based on preliminary phytochemical screening results, the TPHE was analyzed to quantitatively determine flavonoids and phenolic components using LC-MS/MS. The chromatogram is given in **Fig. 3 (a);** relevant details are provided in **Table 2**, Table represents retention time, along with concentrations (g/100ml) of twenty-one bioactive constituents, including phenolic acids and flavonoids. The results indicated that caffeic acid was the most abundant among all bioactive compounds. Caffeic acid is one of the potent reducing, capping, and stabilizing agents that help in green synthesis of NPs, due to presence of a catecholic group that facilitates its adsorption on the metal ions or metal oxides[45].

Table 2. Quantitative estimation of flavonoids and phenolic constituents present in 50% TPHE.

Compound	RT	Response	Concentration	Unit
p-Hydroxybenzoic acid	3.681	47932	0.115	gm/100ml
Protocatechuic acid	3.885	32349	0.0767	gm/100ml
p-Coumaric acid	4.262	8567	0.0543	gm/100ml
Gallic acid	4.359	20395	0.6709	gm/100ml
Caffeic acid	4.445	602451	2.7524	gm/100ml
Ferulic acid	4.445	541994	1.0273	gm/100ml
Sinapic acid	4.619	58587	0.1495	gm/100ml
Chrysin	4.722	17724	0.004	gm/100ml
Naringenin	5.444	854	0.0031	gm/100ml
Naringenin-7-O hexoside	6.168	63862	0.2109	gm/100ml
Pinobanksin	6.387	145600	1.0075	gm/100ml
Kaempferol	9.119	35534	0.0472	gm/100ml
Epicatechin	9.497	72720	0.1631	gm/100ml
Ellagic acid	10.541	32629	0.0918	gm/100ml
Quercetin	11.161	165419	0.6457	gm/100ml
Rhamnetin	11.413	51922	0.1427	gm/100ml
Kaempferol di-O-hexoside	11.539	6992	0.0408	gm/100ml
Quercetin 3-O galactoside	11.747	141649	1.6569	gm/100ml
Kaempferol 3-O glucoside	11.801	37868	0.0661	gm/100ml
Quercetin 3-O rhamnoside	13.2	23322	0.0094	gm/100ml
Rutin	13.566	63104	0.0472	gm/100ml

3.3. Visible Observation of developed NPs

The first indication of the development of ZnO NPs was indicated by a change in visual observation of the solution containing metal precursor (zinc acetate dihydrate), along with 50% TPHE. Initially, the zinc acetate solution (prepared in distilled water) was colorless, while the TPHE solution was orange in shade. When these two components were mixed in the required concentration, the initial color of the mixture appeared brownish-orange. After a specific period, this color transformed into a light, skinny orange (creamy) as shown in **Fig. 3 (b)**. This color change was due to the presence of 21 polyphenolic compounds in 50% TPHE, which was detected by LC-MS/MS. These phytoconstituents of TPHE actively interact with metal ions, reducing them to nanoscale sizes.

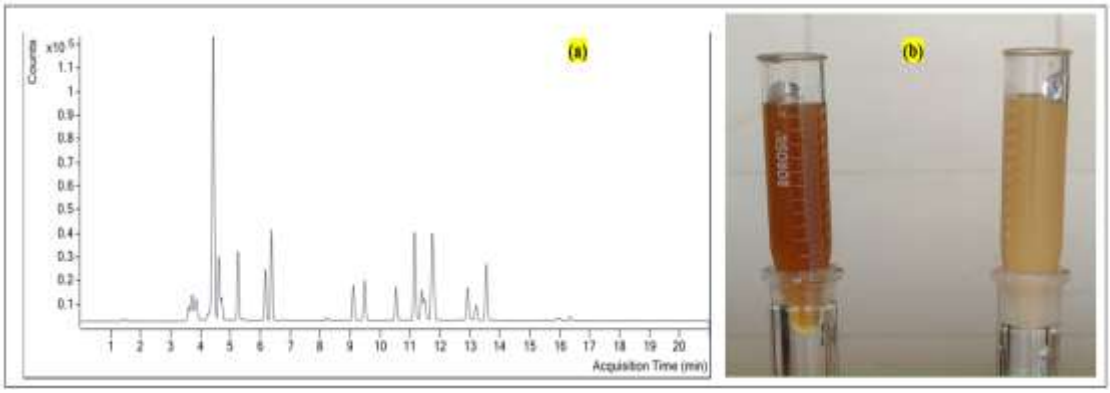

Fig. 3. (a) Representing the LC-MS chromatogram of 50% TPHE. **(b)** Visible color change of the solution at the beginning of the reaction and after successful development of ZnO NPs.

3.4. Optimization of green NPs

The optimization of ZnO NPs yield was decided by adjusting the metal precursor concentration from 0.001 M to 2 M, extract concentration (5 ml to 25 ml), and time (30 minutes to 2 hours). Each set of ZnO NP solutions was centrifuged, and then the pellets were taken out and mixed with 50% hydroalcoholic solvent to measure the absorbance.

3.4.1. Effect of metal precursor concentration

To determine the concentration effect of metal precursor on the yield of NPs, different concentrations varying from 0.001 M to 0.2 M were chosen. The UV-Vis spectra were shown in **Fig. 4 (b)** suggested that maximum absorbance was observed at 0.1 M, indicating a higher yield of ZnO NPs at this specified concentration. It was noticed that upon increasing concentration from 0.001 to 0.1 M, absorbance was increased, but after exceeding this concentration range (at 0.2 M), absorbance decreased. This was due to the production of larger-sized NPs rather than the expected size. Hence, it was concluded that at higher metal precursor concentrations, MONPs exhibited lower absorbance. The obtained results

significantly highlight the metal ion concentration effect on the NPs production yield and to attainment of nano-sized particles.

3.4.2. Effect of TPHE volume

The UV-Vis spectra shown in **Fig. 4 (c)** verified the effect of TPHE volume on the biosynthesis of ZnO NPs. It was achieved by increasing the TPHE volume from 5 mL to 25 mL and maintaining other parameters constant. **Fig. 4 (c)** illustrates the rise in absorbance as the volume of TPHE increased from 5 mL to 20 mL during biosynthesis of NPs. This might be due to the continuous reduction of metal ions into NPs by TPHE. However, a further increase in TPHE volume beyond 20 mL caused a reduction in the absorbance. The reason could be the binding of excess bioactive constituents to the ZnO NPs surface. At higher TPHE concentrations, the solution becomes murky due to the presence of excess bioactive constituents, resulting in decreased absorption intensity. The optimal TPHE volume, finalized for the production of ZnO NPs, was 20 ml.

3.4. Effect of Time

To understand the time-dependent kinetics of ZnONPs biosynthesis, Different time intervals have been selected to check whether the synthesis was going in the right direction. A similar procedure has been followed each time with different time intervals, such as 30 minutes, 1 h, 1.5 h, and 2 h, and then absorbance was measured by using UV-Vis spectra. **Fig. 4 (d)** demonstrates how the time interval affects the biosynthesis of ZnO NPs. An intense absorbance peak was observed at 1 h, and after increasing or decreasing the time above or below 1 h leads to a decrease in absorbance. This might be due to enlarged particle size or changes in crystal structure upon prolongation of the reaction time. Previous investigations on *Monsoon longifolium* leaf extract have shown an absorption peak at 1 h, which is consistent with our findings [46].

3.5. Characterization of green ZnO NPs

3.5.1. UV-Visible Analysis

UV-Vis spectroscopic study of biosynthesized NPs utilizing 50% TPHE exhibited an absorption peak around 368 nm, as shown in **Fig. 4 (a).** A few recently reported studies supported this absorption range (350-380 nm) for developed ZnO NPs [47] by other plant extracts. This was a positive indication of the successful synthesis of ZnO NPs facilitated via phytoconstituents existing in 50% TPHE. Moreover, no additional peaks appeared in the spectrum, confirming the absence of organic contaminants or unreacted metal precursors in the synthesized ZnO NPs, which means they were pure. The slight narrowing of the absorption band suggested a uniform distribution of particle size, due to the stabilizing effects provided by the phytoconstituents present in TPHE. For TPHE, the absorption band was observed between 200 nm to 300 nm, representing the electronic transition of various phenolic and flavonoid compounds present in TPHE. It showed negligible peaks in visible regions[48]

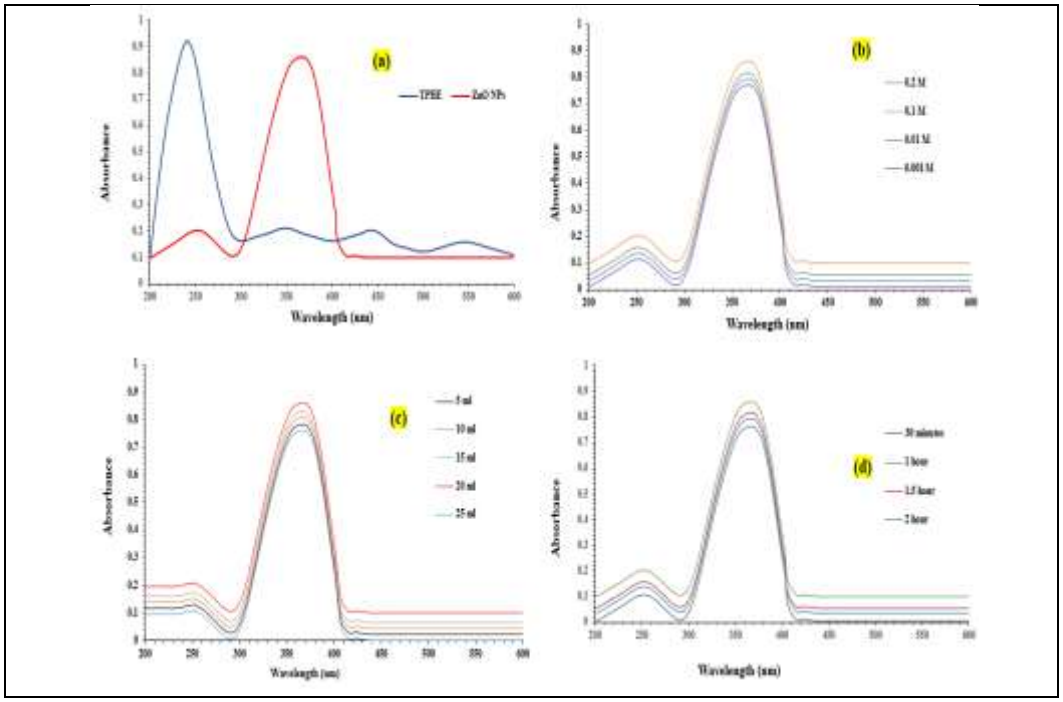

Fig 4. (a) The UV-Vis absorbance spectra of developed ZnO NPs and 50% TPHE (b) representing metal precursor concentration influence on the development of ZnO NPs, (c) 50 % TPHE concentration impact on the production of NPs, (d) Representation of different time intervals effect on the ZnO NPs synthesis.

3.5.2. Zeta Sizer Investigation

Zeta Sizer was utilized to detect the average particle size of developed suspended NPs or to characterize their size distribution and surface charge (zeta potential) [49]. These parameters are critical in determining the stability and dispersibility of the NPs. **Fig 5 (a) demonstrated** 94.26 nm of average particle size and exhibited a size distribution range of 104.2 +-33.5 nm. The size of particles significantly influences biodistribution, tissue uptake, and applicability in the biomedical field. Small size NPs improved penetration power, and facilitates their movement through systemic circulation, allowing them to access the targeted site easily. The polydispersity index (PDI) was 0.100, indicating that the biosynthesized ZnO NPs are relatively monodisperse, with peak intensity recorded at 100%[50].

3.5.3. Zeta Potential analysis

The zeta potential is one of the essential characterization techniques for assessing colloidal stability of the NPs. Zeta potential, showing high magnitude, whether positive or negative, which suggests that the NPs are more likely to remain stable in suspension. This stability prevents aggregation, by causing electrostatic repulsion between particles. Such stability is important in biological and environmental applications, as particle aggregation can reduce effectiveness and alter behaviour. In our measurements, the zeta potential of the developed NPs was -19.9 mV, suggesting a high degree of colloidal stability, as shown in **Figure 5 (b).** This negative charge on the NP's surface helps prevent their aggregation by promoting greater repulsion between the particles, thereby enhancing the stability of ZnO NPs and minimizing agglomeration in the medium. This high zeta potential indicates that the NPs are likely to remain stable over time, which is crucial for their application in biomedical formulations[51].

3.5.4. XRD Examination

XRD analysis of developed ZnO NPs, demonstrated a distinct crystalline structure, featuring well-defined peaks that link to the hexagonal wurtzite phase. As illustrated in **Fig. 5 (c),** notable diffraction peaks appear at a 2θ angle of approximately 31.553º, 34.208º, 36.029º, 47.348º, 56.391º, 62.650º, 66.182º, and 67.750º. 68.870º, 72.36º, and 76.75º. These peaks were allotted to (100), (002), (101), (102), (110), (103). (220), (112), (200), (004), and (202) diffraction planes, confirming the successful production of green NPs. The peak's clarity and intensity. suggests that developed ZnO NPs are free from impurities and possess a crystalline nature. This purity can be linked to the effective capping and reducing effects of the bioactive compounds found in TPHE. Furthermore, with the help of the Scherrer equation, average crystallite size for prominent peaks was determined as 21.93 nm to reinforcing the assertion of nanoscale dimensions. [52,53].

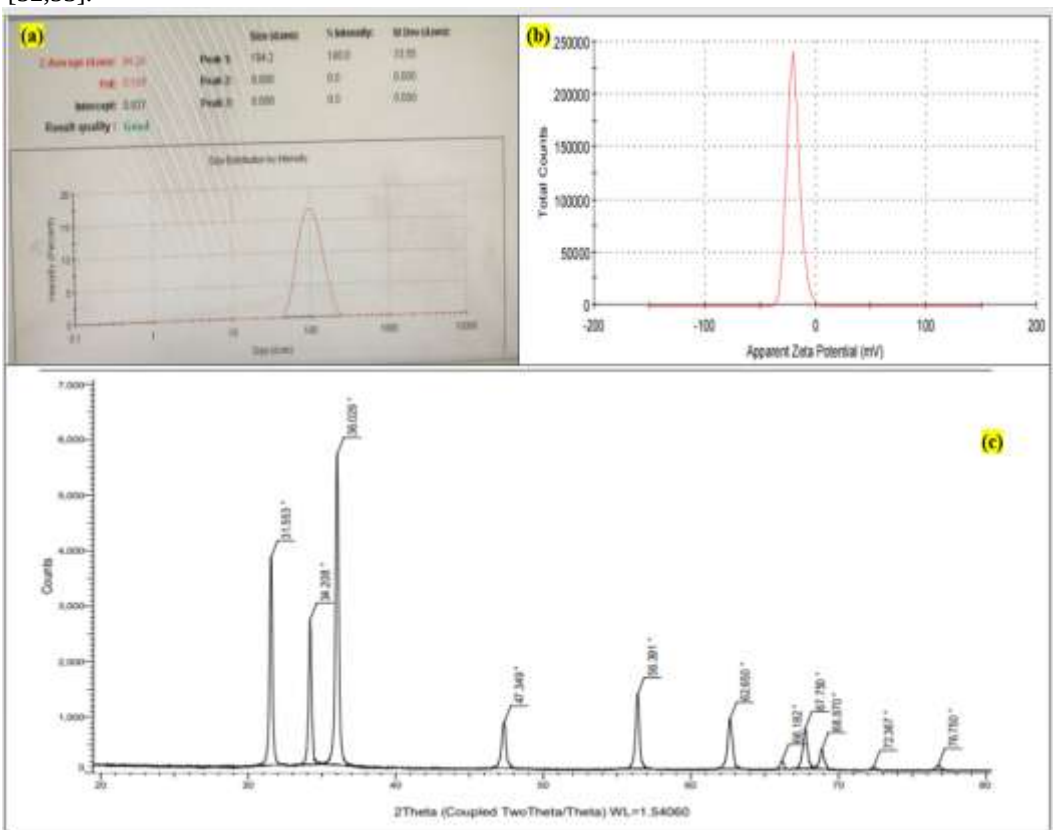

Fig. 5. (a) Determination of particle size by zeta sizer, **(b)** Zeta potential examination of ZnO NPs, **(c)** XRD spectrum of developed ZnO NPs by 50% TPHE.

3.5.5. SEM with EDS analysis

In this study, SEM combined with EDS technology, which simultaneously detects the morphology and elemental composition of the developed ZnO NPs. The SEM pictures revealed a spherical shape with a narrow size distribution, typically ranging from 80.00 nm to 106.87 nm in diameter. The surface morphology appeared slightly smooth, and some particles were agglomerated as shown in **Fig. 6 (a) &(b)**, likely due to the binding capacity of phytochemicals that act as a capping agent that were exist in the TPHE or as a result of particle aggregation during the SEM measurement[54,55].

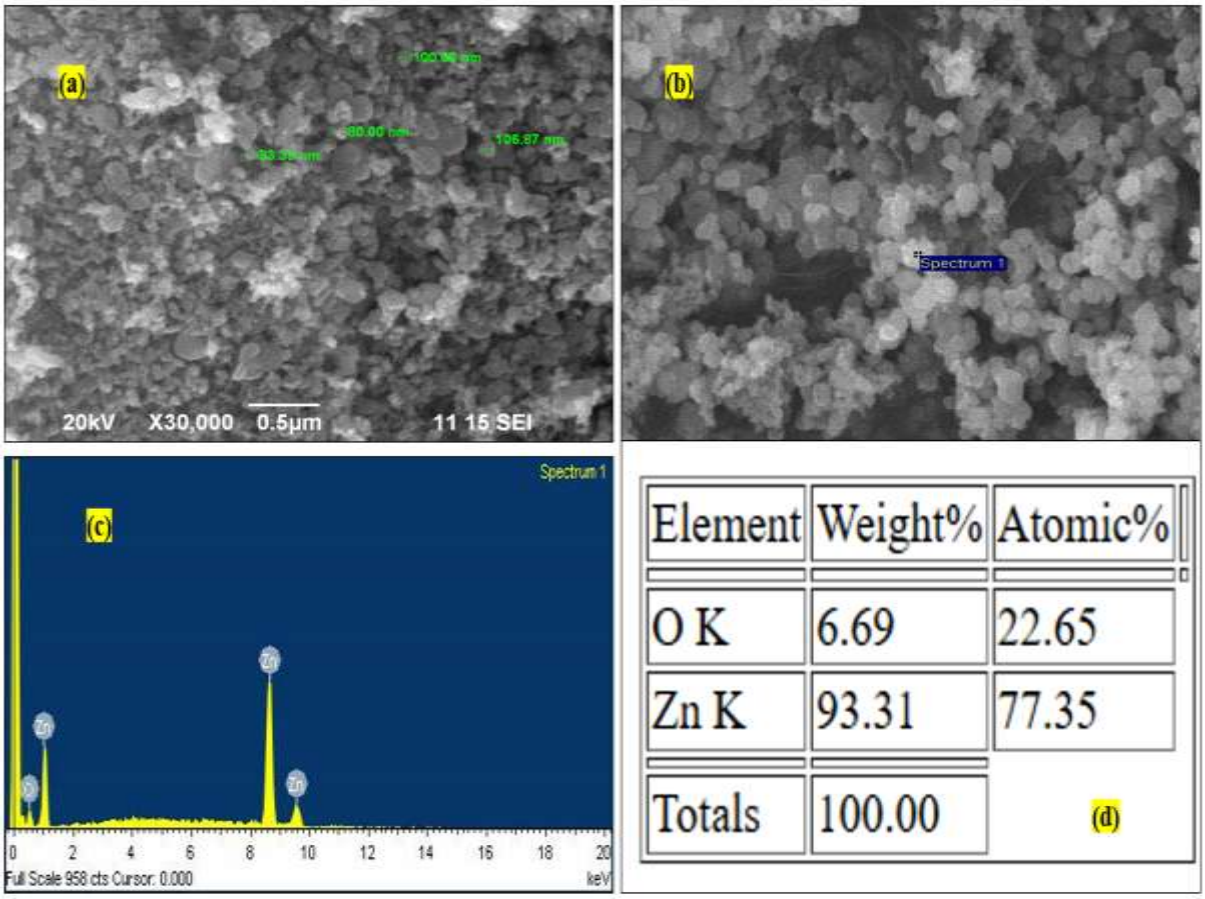

Fig. 6. (a) SEM pictograph of developed ZnO NPs **(b)** SEM picture selected for EDS analysis, **(c)** EDS analysis spectra, **(d)** Detected elements details of synthesized ZnO NPs, details of atomic and weight percentage.

The EDS analysis provided complementary information by confirming the elements present in the ZnO NPs. The EDS spectra have been shown in **Fig. 6 (c)** and display strong peaks of zinc (Zn) and oxygen (O), which are the prime elements of ZnO. **Fig. 6 (d)** shows the mass percent of Zn and O, which is 93.31% and 6.69%, or in total, it is 100%. The atomic percent of Zn to O is 77.35% and 22.65%, respectively, indicating the successful production of pure NPs[56]The absence of significant peaks for other elements in the EDS spectra confirmed that the biosynthesized NPs were free from major impurities or contaminants. The SEM and EDS spectra revealed that the biosynthesized NPs have high elemental purity and spherical morphology.

3.5.6. TEM Investigation

The TEM examination provided detailed insights into the size and shape of biosynthesized ZnO NPs. **Fig. 7 (a)** represents ZnO NPs TEM image, which indicates that ZnO NPs are primarily spherical, monodisperse, and scattered nonuniformly, along with a few aggregated particles[57]. The particle size is about 68.4 nm, indicating the successful formation of ZnO NPs.

3.5.7. FTIR analysis

The FTIR spectrum of developed NPs has been represented in **Fig. 7 (b)**. The spectrum showed characteristic peaks of various functional groups required for the metal precursor reduction and converted into desired NPs. A strong peak appeared around 3445.5 cm^{-}1, which confirms O-H groups, attributed to phenolic compounds and flavonoids in the TPHE [58]. The small distinct peak observed at 2092.1 cm^{-1} represented the presence of C–H stretching vibrations of the aromatic compounds[59]. A little intense absorption band appeared at 1637.7 cm^{-1} is due to C=O stretching vibrations, which may arise from the carbonyl group of proteins and polyphenolic components available in the extract and those that interact with the ZnO NPs surface[48]. This peak also represents the C=C stretching vibrations in the aromatic compound

(cyclic alkenes)/N-H bending vibrations of the amine group found in proteins. The peaks at 1013.1 cm^{-1} denote C–O–C stretching vibrations of polysaccharides and C=C–O bonds of phenolic moieties, likely due to the presence of alcohol or ester in the extract. The peaks visible between 1000 to 950.0 cm^{-1} are due to C=C and C-H bending, representing aromatic and alkenes(extract)[60]. Lastly, the broad peaks observed at 594.4 cm^{-1} signify the stretching of Zn-O, verifying the formation of ZnO NPs. These FTIR results highlighted the potential phytoconstituents' role in reducing and stabilizing the process of developing ZnO NPs[61].

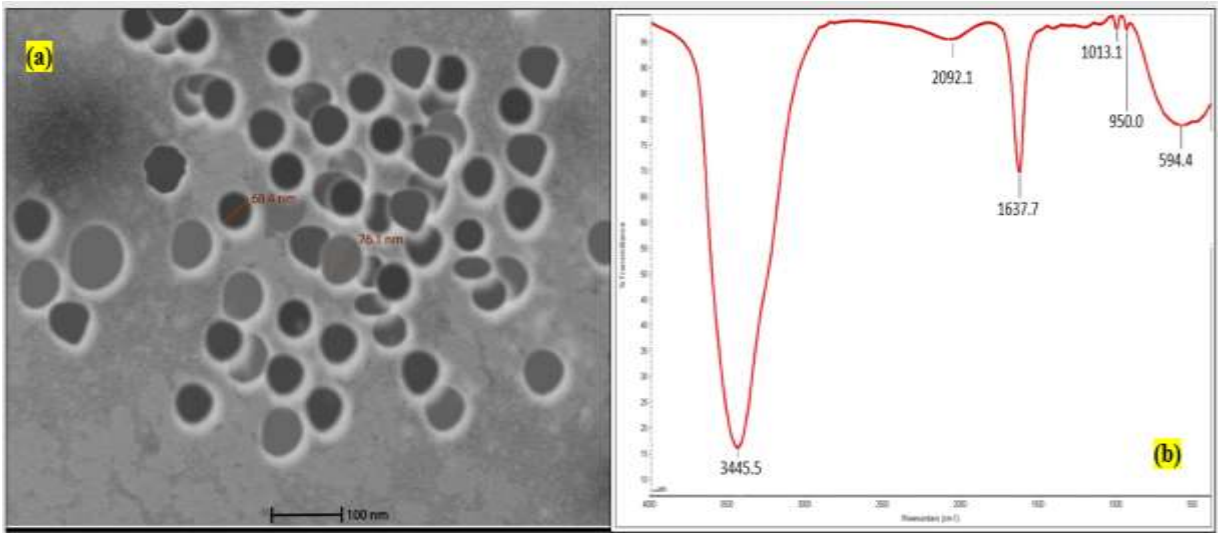

Figure 7. (a) TEM image of TPHE-mediated ZnO NPs, **(b)**FTIR spectrum of TPHE-mediated ZnO NPs.

3.6. Biological actions

3.6.1. Antioxidant potential

This research explored the antioxidant potential of green ZnONPs and TPHE by utilizing DPPH, FRAP, and ABTS assays. All these methods are based on the capacity to scavenge dangerous free radicals. “Ascorbic acid” (standard) ’s antioxidant potential was an optimistic reference for comparative analysis. The results were demonstrated as percent inhibition concerning control at different strengths (0.78, 1.56, 3.125, 6.25, 12.5, 25, and 50 µg/ml), represented in the graphs in **Fig. 8a, 8b & 8c**. Among all three antioxidant assays, the FRAP test showed the highest antioxidant capacity for synthesized ZnO NPs, possessing a minimal IC_{50} value comparable to standard ascorbic acid. IC_{50} is the minimal inhibitory concentration to diminish 50 % of the dangerous free radicals. The minimum IC_{50} value represents maximum antioxidant potency.

3.6.1.1. FRAP activity

FRAP activity was carried out to measure the ferric-reducing capability of both ZnO NPs and TPHE, along with the standard drug ascorbic acid, at various concentrations. 10µl from each sample was taken and added to a mixture that contains sodium phosphate buffer (0.2 M) and potassium ferricyanide (1%). Further, it was placed for 20 minutes in an incubator at 50°C. Following the incubation, a blue color (ferrous-tripyridyl triazine) complex was formed after adding ferric chloride and trichloroacetic acid, which was then detected with a microplate reader at 700 nm. The antioxidants in the sample reduce ferric ions to ferrous ions, which causes the color shift. The color’s intensity shows the degree of antioxidant activity; the higher intensity of the color correlates with greater absorbance and, therefore, a higher antioxidant-reducing power. **Fig. 8 (a)** represents concentration-dependent antioxidant activity for developed ZnO NPs, their related TPHE, and standard drug ascorbic acid. ZnO NPs demonstrated strong antioxidant potential among both TPHE and ZnO NPs, with an IC_{50} value of 10.48 ± 0.05 µg/ml, closer to standard drug ascorbic acid, having an IC_{50} of 7.373 ± 0.05 µg/ml. However, TPHEs showed lower $IC_{50,}$ 28.16 ± 0.05 µg/ml, representing greater antioxidant activity than produced by ZnO NPs. As a result, the produced ZnO NPs demonstrated their potential as natural antioxidants by exhibiting strong antioxidant activity as per with the standard. Similar antioxidant potential was observed with synthesized ZnO NPs by utilizing aloe vera leaf extract, where developed NPs showed excellent ferric-reducing action compared with the extract alone. This ferric-reducing ability suggests that the compounds are effective electron donors, capable of reducing oxidized intermediates, thus preventing oxidative damage. The FRAP assay results underscore the effectiveness of these compounds in neutralizing free radicals and their potential use in applications where antioxidant properties are required [62].

3.6.1.2. DPPH radical scavenging potential

Since the DPPH assay is a rapid and accurate way to assess the capacity to scavenge free radicals, and is widely used. DPPH is a highly stable purple-colour free radical that is reduced to yellow diphenyl picrylhydrazine when interacting with a substance with antioxidant potential. "% inhibition" was utilized to display the scavenging activity for the control. According to the antioxidant results illustrated in **Fig. 8 (b),** TPHE and green ZnO NPs exhibited concentration-dependent free radical scavenging potential. Antioxidant activity was limited at lower concentrations, while it increased with concentration. The standard compound "Ascorbic acid" displayed maximum scavenging activity (92.67%) with a minimum IC_{50} value of 7.03 ± 0.02 µg/ml when compared to ZnO NPs and TPHE, suggesting its highest antioxidant potential as expected. However, the synthesized ZnO NPs exhibited a 12.37 ± 0.02 µg/ml IC_{50} value, while it was 27.07 ± 0.03 µg/ml for TPHE. Data revealed that ZnO NPs are potent scavengers of antioxidants, as the percentage of scavenging activity is nearly that of ascorbic acid. These results prove that ZnO NPs synthesized using TPHE are an appropriate alternative to conventional antioxidants such as ascorbic acid. Similar results were obtained with *Clerodendrum phlomidis* extract-mediated ZnO NPs, showing increased antioxidant activity by synthesizing ZnO NPs using *Clerodendrum phlomidis* extract[63]. Awan et al. also observed that the *Ailanthus altissima* leaf extract showed lower antioxidant potential when compared to synthesized ZnO NPs, and its antioxidant activity is comparable to standard ascorbic acid[64].

3.6. 1.3. ABTS Assay

The ABTS assay was also performed to measure the antioxidant potential of both green ZnO NPs and TPHE. A decreased absorbance was observed for both samples, suggesting the free radical scavenging activity. Further, the percent inhibition was calculated for both tested samples (ZnO NPs and TPHE) and ascorbic acid (standard for comparison). The results were displayed in **Fig. 8 (c), which** demonstrated a concentration-dependent antioxidant potential for both TPHE and developed NPs. The TPHE showed lower scavenging potential with an IC_{50} of 30.04 ± 0.05 µg/ml when compared with developed NPs. The ZnO NPs displayed significant antioxidant potential with a 12.48 ± 0.03 µg/ml IC_{50} value, and which was quite close to ascorbic acid with an 8.737 ± 0.02 µg/ml IC_{50} value. This enhancement was possible due to the synergistic effect of the extract present in the developed NPs[65].

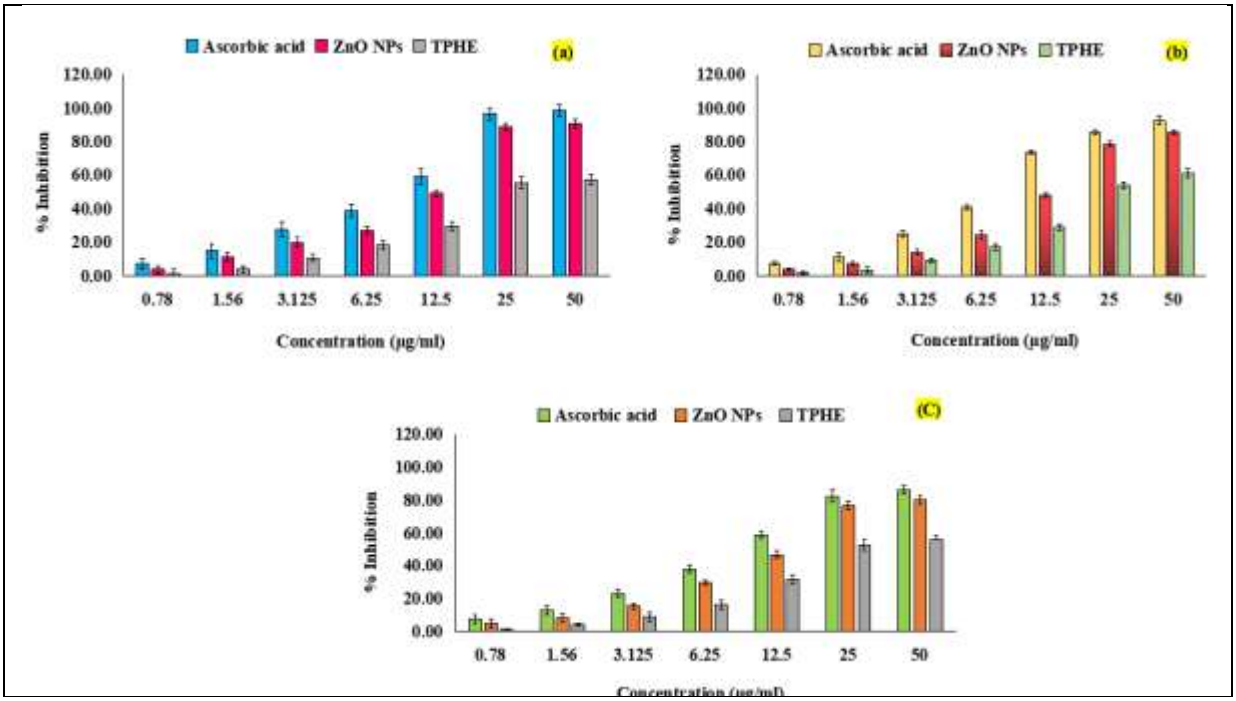

Figure 8. Graphical representation of *in vitro* antioxidant activity in percent inhibition for green ZnO NPs, TPHE, and standard ascorbic acid. **(a)** FRAP activity, **(b)** DPPH activity, and **(c)** ABTS assay data are presented as Mean ± SD (n = 4, P < 0.0001).

3.6.2 Cytotoxicity studies via MTT assay

An MTT assay evaluated the cytotoxicity effects of biosynthesized ZnO NPs, TPHE, and standard drug doxorubicin (as reference) towards SK-OV3, A549, and Vero **cell lines**. Data revealed that developed ZnO NPs exhibited excellent cytotoxic activity towards the SK-OV3 and A549 cancer cell lines, exhibiting an IC_{50} of **20.50 ±0.08** µg/mL and **22.85 ±0.07** µg/mL, respectively, that were closer to the doxorubicin (standard), exhibiting IC_{50} of **10.27 ±0.07** µg/mL and **17.49 ±0.04** µg/mL for the same cancer cell lines. Importantly, these NPs showed reduced cytotoxicity towards Vero

cells, suggesting that green ZnO NPs selectively target cancer cells while displaying minimal effects on normal Vero cells, as shown in **Fig. 9.**

Along with synthesized ZnO NPs, the cytotoxic potential of TPHE was also assessed on the same three tested cell lines at all these specified concentrations: 1.5, 3.125, 6.25, 12.5, 25, 50, 100 µg/mL and 0 were taken as control, and cell viability percentage vs concentration graph was expressed in **Fig. 10a.** TPHE exhibited lower cytotoxic activity towards SK-OV3 and A549 cancer cell lines, with an IC_{50} value 47.62 ±0.04 µg/mL and 63.14 ±0.03 µg/mL, respectively **(Fig. 10 (b & c).** This indicates that THPE has notably lower potency than synthesized ZnO NPs. Additionally, the TPHE displayed minimal cytotoxic activity (maximum cell viability %) towards the Vero cell line, indicating its biocompatibility and potential as a complementary agent in anticancer treatments. This dual approach highlights the promising role of ZnO NPs in selectively targeting cancer cells, particularly ovarian cancer cells, while sparing normal healthy cells. **Table 3** demonstrates the IC_{50} value data of standard drug doxorubicin, ZnO NPs, and TPHE against all three cell lines. These findings suggest that the ZnO NPs prepared in this study are safe for use, exhibiting a low cytotoxic profile on Vero cell lines and showing cytotoxic towards cancer cell lines at the tested concentrations[66][67][68].

Table 3. Demonstrates the IC_{50} value data of ZnO NPs, TPHE, and standard drug doxorubicin against all three tested cell lines (VERO, SK-OV3, and A549).

Tested Cell lines	**IC_{50} Value (µg/mL)**		
	Doxorubicin	**ZnO NPs**	**TPHE**
SK-OV3 cancer cell line	**10.27 ±0.07**	**20.50 ±0.08**	**47.62 ±0.04**
A549 cancer cell line	**17.49 ±0.04**	**22.85 ±0.07**	**63.14 ±0.03**
VERO normal cell line	**25.67±0.06**	**66.46 ±0.05**	**387.2 ±0.04**

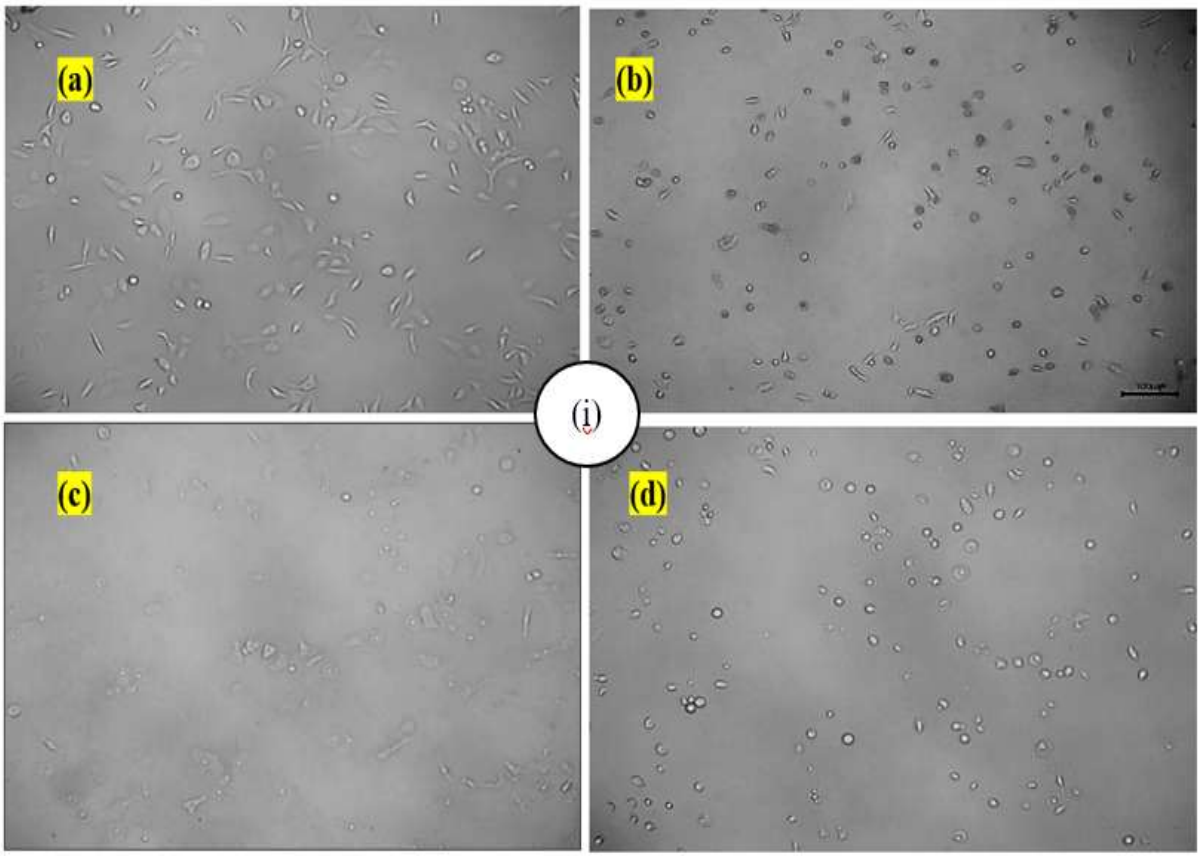

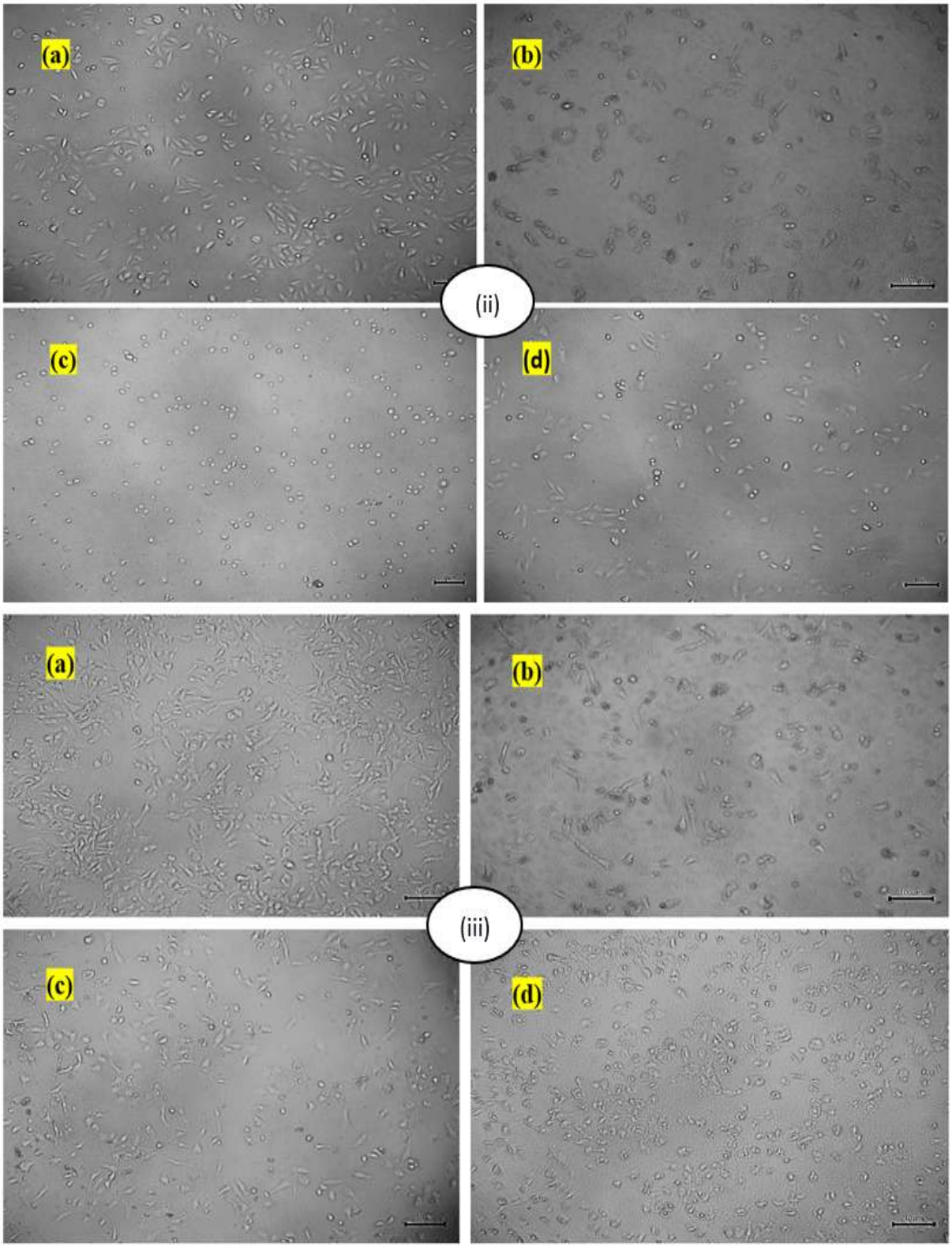

Figure 9. Representing cancer cells inhibition images for (a) control (b) Doxorubicin, (c) ZnO NPs, and (d) TPHE for SKOV-3 cell line (i), A549 cell line (ii), and Vero cells (iii).

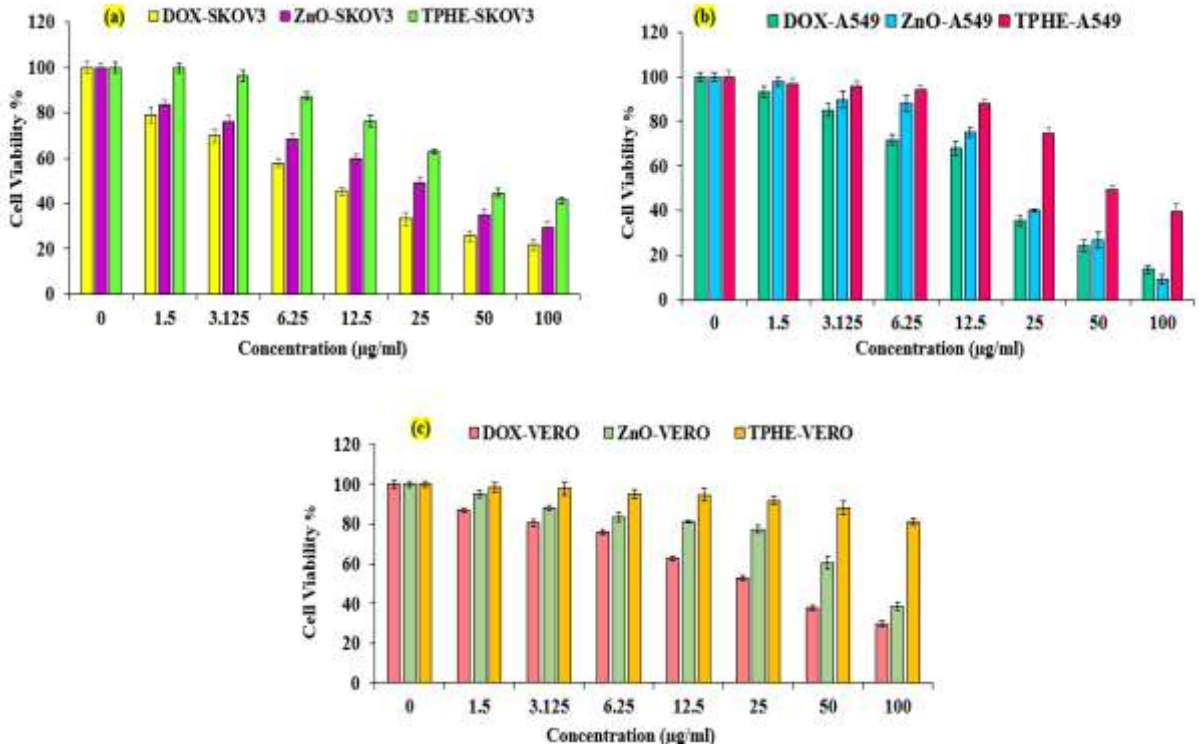

Figure 10. Graphical illustration of cell viability % for standard drug doxorubicin, ZnO NPs, and TPHE against SK-OV3 (a), A549 (b), and VERO (c) cancer cell lines after 24 hours. Bars represented the Mean ± SD (n = 4, P < 0.05).

3.6.3. Antibacterial activity

The assessment of antibacterial potency of both ZnO NPs and TPHE was investigated against selected bacterial strains, which involved: two species of gram-positive bacteria (*B. subtilis* and *E. faecalis*) and two of gram-negative, including *E. coli* and *P. aeruginosa*. The evaluation was conducted using the Zone Inhibition Method (Kirby-Bauer method). 10 µg of standard Ciprofloxacin was taken as a positive control, while DMSO acted as the negative control. The measured inhibitory zone after 24 hours of incubation at the respective concentrations, including 6.25, 12.5, 25, 50, and 100 µg/mL, was represented in **Figure 11**. It was observed that higher concentration of the sample improves inhibitory zones. Based on measured inhibitory zones, it was found that developed NPs displayed moderate antibacterial activity throughout all bacterial strains, and displayed a little stronger effect on gram-positive bacteria. The measured inhibition zones were as follows: 13 mm for *E. faecalis*, 12.5 mm for *E. coli*, 11.4 mm for *P. aeruginosa*, and 10 mm for *B. subtilis* at 100 µg/mL concentration. In contrast, the negative control (DMSO) did not display any inhibitory zone, while the positive control (Ciprofloxacin) demonstrated strong inhibitory zone towards all tested strains, such as 26, 30, 28, and 29 mm for *B. subtilis*, *E. faecalis*, *E. coli*, and *P. aeruginosa* respectively.

In comparison, the antibacterial potency of TPHE was also tested under the same experimental conditions. However, TPHE demonstrated lower antibacterial effects against all tested bacterial species; its inhibition zone was notably smaller when compared with developed ZnO NPs, as shown in **Table 4**. The overall result suggested that *E. faecalis* was the most sensitive to ZnO NPs, followed by *E. coli*, whereas TPHE exhibited lower antibacterial activity in comparison to ZnO NPs. In contrast, the Gram-positive strain, *B. subtilis*, showed relatively lower susceptibility to ZnO NPs and the TPHE. This comparative analysis highlights the superior antibacterial action of developed NPs, particularly against Gram-positive pathogens, which is due to the synergistic activity of the peel phytoconstituents utilized for the production of ZnO NPs[65]. The antibacterial action of developed NPs towards multiple bacteria can be explained by their direct interaction with bacterial membranes. The NPs penetrate the e bacterial membrane through small pores. Their small size allows for direct or electrostatic interaction with the cell membrane, leading to internalization, resulting in active oxygen species production. Hypotheses also explained that ZnO NPs disrupt bacterial cell membranes more effectively, resulting in increased permeability and subsequent cell death [70].

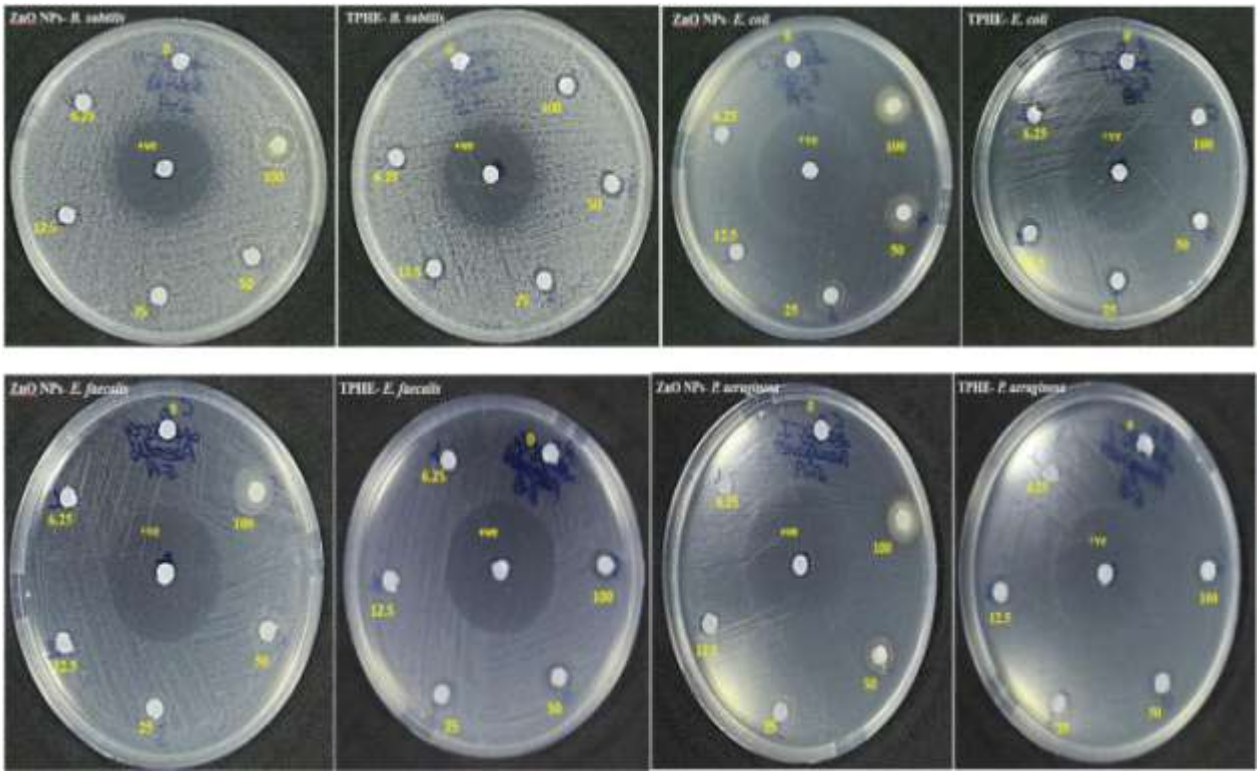

Figure 11. Displaying inhibitory zones using the disc diffusion method for developed ZnO NPs and TPHE towards gram-positive and negative bacteria. Where 10µg Ciprofloxacin is used as a standard positive control. Each disc contained 10 µl of sample concentration strength (6.25, 12.5, 25, 50, and 100 µg/mL), and DMSO served as a negative control. All tests were conducted in triplicate.

Table 4. Inhibitory Zone (mm) of TPHE, and developed ZnO NPS against test microorganisms. The data is displayed as Mean ± **SD (**n = 3, P < 0.05).

Concentrations in (µg/mL)	**Zone of Inhibition (mm) Mean ± SD (n=3)**			
ZnO NPs	**Gram-positive bacteria**		**Gram-negative bacteria**	
	B. subtilis	***E. faecalis***	***E. coli***	***P. aeruginosa***
*Ciprofloxacin	26	30	28	29
0 (DMSO)	0	0	0	0
6.25	6	6	6.3 ± 0.5	6
12.5	6	6	7	7
25	7	8	10	8
50	8	11	11	9
100	10	13	12.5 ± 0.1	11.4± 0.2
TPHE				
*Ciprofloxacin	26	27	28	28
0 (DMSO)	0	0	0	0
6.25	6.2 ± 0.1	6.2± 0.1	6.5± 0.5	6.2± 0.1
12.5	7	6	8	7
25	7	6	8	7
50	8	8	7	7
100	8	9	10	9

* Ciprofloxacin (10 µg) and DMSO were positive and negative controls.

CONCLUSION

This research highlights the importance of green synthesis in nanotechnology, as it reduces the harmful environmental impact associated with traditional physico-chemical methods. ZnO NPs were developed by utilizing 50% hydroalcoholic extract of the peel from T. natans is a renewable and sustainable source. This extract contains various polyphenolic constituents and flavonoids, which contribute to the synthetic process and biological activity of ZnO NPs. After synthesis, characterization was performed using several techniques, including UV-Vis spectroscopy, zeta sizer, zeta potential, XRD, FTIR, SEM with EDS, and TEM,

which revealed that NPs were of accurate size and shape. Further antioxidant potential was determined by FRAP, ABTS, and DPPH assays. Data indicated that the antioxidant activity of the developed NPs was dose-dependent and superior to that of pure TPHE. NPs smaller size enhance surface area and reactivity, leading to more efficient electron transfer by the ZnO NPs. This, in turn, enhanced the reducing power observed in the antioxidant assays.

Moreover, NPs were explored against their anticancer activity via the MTT assay. The results of anticancer activity demonstrated a higher percentage of cytotoxicity by ZnO NPs against SK-OV3 cell lines than against A549 cell lines. The anticancer action of developed NPs was higher than pure TPHE, which revealed the potential of ZnO NPs to alleviate cancer. They also displayed low cytotoxicity on normal Vero cells, which showed the safety of green ZnO NPs. The observed level of selectivity was due to bioactive constituents present in TPHE, which would augment the biocompatibility profile of the ZnO NPs.

Along with anticancer potential, ZnO NPs also showed remarkable antibacterial activity. ZnO NPs exhibited a more significant zone of inhibition than pure TPHE, demonstrating the advantageous feature of the synthesis of NPs. The enhanced antibacterial activity is due to the production of reactive oxygen species, Zn^{2+} ions release at the bacterial site which leads to damage in cellular membrane resulting cell death. Due to this, ZnO NPs are the most efficient natural antibacterial agent. The cost-effectiveness and simplicity of the entire method make it appropriate for large-scale synthesis and open numerous avenues in the biomedical field. Conclusively, the ZnO NPs exhibited significant antioxidant, anticancer, and antibacterial properties; which makes them a great option to use in pharmaceutical applications. This study throws light on the utilization of agricultural waste (peel)in producing green ZnO NPs. It provides future breakthroughs in nanomedicine, especially in treating bacterial infections and cancers.

5. Future prospective

This finding holds significant potential for the eco-friendly ZnO NPs, which will be explored further for various biomedical applications. Future studies will target in vivo animal testing to verify the antibacterial and anticancer properties of these NPs, as well as assess their long-term effectiveness in living organisms. It is also essential to expand a better understanding of the mechanisms behind their specific cytotoxicity towards malignant cells while ensuring minimum toxicity towards normal cells. Furthermore, NPs will be investigated in combination with other drugs to achieve synergistic effects, and modifications to their surfaces may be made for targeted therapy, which could enhance therapeutic outcomes. Finally, consistent research on the long-term toxicity of the green synthesis process is necessary to ensure sustainability and reproducibility.

Credit authorship contribution statement

Swati Dubey: Writing- original draft. Yogendra Singh: Supervision, and editing. Shiv Kumar Yadav: Resources. Tarun Virmani: Supervision, Writing, and editing. Ashwani Sharma: Conceptualization, data curation. Mahima Chauhan: Visualization

Consent to Publish Declaration

Not applicable

Ethics and Consent to Participate Declarations

Not applicable

Declaration of competing interest

On behalf of all authors, the corresponding author states that there is no conflict of interest.

REFERENCES

1. Kumar G, Virmani T, Sharma A, Pathak K. Codelivery of Phytochemicals with Conventional Anticancer Drugs in Form of Nanocarriers. Pharmaceutics. 2023;15:889.
2. Kumar G, Virmani T, Chhabra V, Virmani R, Pathak K, Akhtar MS, et al. Transforming cancer treatment: The potential of nano nutraceuticals. International Journal of Pharmaceutics. 2024;667:124919.
3. Romero-Trejo D, Aguiñiga-Sanchez I, Ledesma-Martínez E, Weiss-Steider B, Sierra-Mondragón E, Santiago-Osorio E. Anti-cancer potential of casein and its derivatives: novel strategies for cancer treatment. Med Oncol. 2024;41:200.
4. Kumar G, Jain P, Virmani T, Sharma A, Akhtar MS, Aldosari SA, et al. Enhancing therapy with nano-based delivery systems: exploring the bioactive properties and effects of apigenin. Therapeutic Delivery. 2024;15:717–35.
5. Kumar NR, Balraj TA, Kempegowda SN, Prashant A. Multidrug-Resistant Sepsis: A Critical Healthcare Challenge. Antibiotics. 2024;13:46.
6. Salah M, Elkabbany NAS, Partila AM. Evaluation of the cytotoxicity and antibacterial activity of nano-selenium prepared via gamma irradiation against cancer cell lines and bacterial species. Sci Rep. 2024;14:20523.
7. Shandhiya M, Janarthanan B, Sharmila S. A comprehensive review on antibacterial analysis of natural extract-based metal and metal oxide NPs. Arch Microbiol. 2024;206:52.
8. Vo TS, Jeon B, Nguyen VPT, Hoang T, Lwin KM, Han S, et al. A comprehensive review of laser processing-assisted 2D functional materials and their specific applications. Materials Today Physics. 2024;47:101536.
9. Dubey S, Virmani T, Yadav SK, Sharma A, Kumar G, Alhalmi A, et al. Breaking Barriers in Eco-Friendly Synthesis of Plant-Mediated Metal/Metal Oxide/Bimetallic NPs: Antibacterial, Anticancer, Mechanism Elucidation, and Versatile Utilizations. J Nanomaterials [Internet]. 2024 [cited 2024 Oct 28];2024. Available from: https://doi.org/10.1155/2024/9914079

10. Vijayaram S, Razafindralambo H, Sun Y-Z, Vasantharaj S, Ghafarifarsani H, Hoseinifar SH, et al. Applications of Green Synthesized Metal NPs — a Review. Biol Trace Elem Res. 2024;202:360–86.
11. Al-darwesh MY, Ibrahim SS, Mohammed MA. A review on plant extract mediated green synthesis of zinc oxide NPs and their biomedical applications. Results in Chemistry. 2024;7:101368.
12. Adra HJ, Ryu H, Jo A, Lee J, Choi S-J, Kim Y-R. Ligand-based magnetic extraction and safety assessment of zinc oxide NPs in food products. Journal of Hazardous Materials. 2024;465:133235.
13. Manimegalai P, Selvam K, Loganathan S, Kirubakaran D, Shivakumar MS, Govindasamy M, et al. Green synthesis of zinc oxide (ZnO) NPs using aqueous leaf extract of Hardwickia binata: their characterizations and biological applications. Biomass Conv Bioref. 2024;14:12559–74.
14. Zöngür A, Er Zeybekler S. Evaluation of the effects of zinc oxide (ZnO NPs) NPs synthesized by green synthesis on Caenorhabditis elegans. BIOLOGIA FUTURA [Internet]. 2024 [cited 2024 Oct 17]; Available from: https://doi.org/10.1007/s42977-024-00217-3
15. Tiwari AK, Jha S, Tripathi SK, Shukla R, Awasthi RR, Bhardwaj AK, et al. Spectroscopic investigations of green synthesized zinc oxide NPs (ZnO NPs): antioxidant and antibacterial activity. Discov Appl Sci. 2024;6:399.
16. Mohamad Sukri SNA, Shameli K, Mei-Theng Wong M, Teow SY, Chew J, Ismail NA. Cytotoxicity and antibacterial activities of plant-mediated synthesized zinc oxide (ZnO) NPs using Punica granatum (pomegranate) fruit peels extract. Journal of Molecular Structure. 2019;1189:57–65.
17. Alyamani AA, Albukhaty S, Aloufi S, Almalki FA, Al-Karagoly H, Sulaiman GM. Green fabrication of zinc oxide NPs using phlomis leaf extract: Characterization and in vitro evaluation of cytotoxicity and antibacterial properties. Molecules. 2021;26.
18. Li J, Li Y, Wu H, Naraginti S, Wu Y. Facile synthesis of ZnO NPs by Actinidia deliciosa fruit peel extract: Bactericidal, anticancer and detoxification properties. Environmental Research. 2021;200.
19. Antimicrobial E, Activities P, Al-askar AA, Hashem AH, Elhussieny NI, Saied E. Green Biosynthesis of Zinc Oxide NPs Using Pluchea. Molecules. 2023;
20. Elbrolesy A, Abdou Y, Elhussiny FA, Morsy R. Novel Green Synthesis of UV-Sunscreen ZnO NPs Using Solanum Lycopersicum Fruit Extract and Evaluation of Their Antibacterial and Anticancer Activity. Journal of Inorganic and Organometallic Polymers and Materials. 2023;33:3750–9.
21. Ghaffar S, Abbas A, Naeem-ul-Hassan M, Assad N, Sher M, Ullah S, et al. Improved Photocatalytic and Antioxidant Activity of Olive Fruit Extract-Mediated ZnO NPs. Antioxidants. 2023;12.
22. Islam MF, islam S, Miah MAS, Huq AKO, Saha AK, Mou ZJ, et al. Green synthesis of zinc oxide nano particles using Allium cepa L. waste peel extracts and its antioxidant and antibacterial activities. Heliyon. 2024;10:e25430.
23. Hussien NA, Al Malki JS, Al Harthy FAR, Mazi AW, Al Shadadi JAA. Sustainable Eco-Friendly Synthesis of Zinc Oxide NPs Using Banana Peel and Date Seed Extracts, Characterization, and Cytotoxicity Evaluation. Sustainability. 2023;15:9864.
24. Kanase DV, Gupta A, Patil K, Bandarkar A, Khan DM. Water chestnut (Trapa natans L.): Nutritional, phytochemical and pharmacological aspects (An Overview). J Pharmacogn Phytochem. 2024;13:46–50.
25. Rehman AU, Khan AU, Sohaib M, Rehman H. Comparative Analysis of Nutritional Properties, Phytochemical Profile, and Antioxidant Activities between Red and Green Water Chestnut (Trapa natans) Fruits. Foods. 2024;13:1883.
26. Din GMU, Hussain A, Ashraf H, Kausar T, Fatima H, Sidrah, et al. Physicochemical, nutritional and organoleptic characteristics of cookies based on water chestnut (Trapa natans) and wheat. Food Chemistry Advances. 2024;4:100691.
27. Hashem AH, El-Sayyad GS. Antimicrobial and anticancer activities of biosynthesized bimetallic silver-zinc oxide NPs (Ag-ZnO NPs) using pomegranate peel extract. Biomass Conv Bioref. 2024;14:20345–57.
28. Al-Khaial MQ, Chan SY, Abu-Zurayk RA, Alnairat N. Biosynthesis and Characterization of Zinc Oxide NPs (ZnO-NPs) Utilizing Banana Peel Extract. Inorganics. 2024;12:121.
29. Shaikh JR, Patil M. Qualitative tests for preliminary phytochemical screening: An overview. Int J Chem Stud. 2020;8:603–8.
30. M G, T B, A S, S S, N S, T V, et al. In Vitro Phytochemical Screening, Cytotoxicity Studies of Curcuma longa Extracts with Isolation and Characterisation of Their Isolated Compounds. Molecules (Basel, Switzerland) [Internet]. 2021 [cited 2024 Nov 25];26. Available from: https://pubmed.ncbi.nlm.nih.gov/34946592/
31. Benouchenne D, Bellil I, Akkal S, Bensouici C, Khelifi D. LC-MS/MS analysis, antioxidant and antibacterial activities of Algerian fir (Abies numidica de LANNOY ex CARRIÈRE) ethylacetate fraction extracted from needles. Journal of King Saud University - Science. 2020;32:3321–7.
32. Iheme CI, Elemike EE, Igwe CU, Ujowundu FN, Ogbonna CU, Uche ZC, et al. Synthesis, characterization, radical scavenging properties of zinc oxide NPs and inhibitory effect of ZnONPs-ciprofloxacin nanoconjugates on multidrug-resistant Staphylococcus aureus (MRSA) enzyme. Inorganic Chemistry Communications. 2024;160:111864.
33. Kumar A, Singh AL, Rajak PK, Kumar A, Singh PK. Beneficiation of High Sulfur Tertiary Coal of Assam with Burkholderia sp. GR 8-02. An Eco-Friendly Approach Toward Clean Coal Production. Geomicrobiology Journal. 0:1–12.
34. Rashid MU, Shah SJ, Attacha S, Khan L, Saeed J, Shah ST, et al. Green Synthesis and Characterization of

Zinc Oxide NPs Using Citrus limetta Peels Extract and Their Antibacterial Activity Against Brown and Soft Rot Pathogens and Antioxidant Potential. Waste Biomass Valor. 2024;15:3351–66.
35. Bekele SG, Ganta DD, Endashaw M. Green synthesis and characterization of zinc oxide NPs using Monoon longifolium leave extract for biological applications. Discov Chem. 2024;1:5.
36. Kumar G, Virmani T, Pathak K, Kamaly OA, Saleh A. Central Composite Design Implemented Azilsartan Medoxomil Loaded Nanoemulsion to Improve Its Aqueous Solubility and Intestinal Permeability: In Vitro and Ex Vivo Evaluation. Pharmaceuticals (Basel). 2022;15:1343.
37. Ravichandran V, Vasanthi S, Shalini S, Shah SAA, Tripathy M, Paliwal N. Green synthesis, characterization, antibacterial, antioxidant and photocatalytic activity of Parkia speciosa leaves extract mediated silver NPs. Results in Physics. 2019;15:102565.
38. Inam M, Haider Z, Anjum S, Soliman MM, Ahmad B, Hussain MI, et al. Differential impact of biogenic and chemically synthesized zinc oxide NPs on anti-aging, anti-oxidant and anti-cancerous activities: a mechanism based study. New J Chem. 2024;48:10161–76.
39. Arulvendhan V, Saravana Bhavan P, Rajaganesh R. Molecular Identification and Phytochemical Analysis and Bioactivity Assessment of Catharanthus roseus Leaf Extract: Exploring Antioxidant Potential and Antimicrobial Activities. Appl Biochem Biotechnol [Internet]. 2024 [cited 2024 Nov 25]; Available from: https://doi.org/10.1007/s12010-024-04902-w
40. Raphael R, Aswathy WF, Anila EI. In vitro cytotoxicity studies of Ga2O3 microstructures on L929 and MCF-7 cell lines using MTT assay. MRS Communications [Internet]. 2024 [cited 2024 Nov 25]; Available from: https://doi.org/10.1557/s43579-024-00647-z
41. Hayat K, Din IU, Alam K, Khan FU, Khan M, Mohamed HI. Green synthesis of zinc oxide NPs using plant extracts of Fumaria officinalis and Peganum harmala and their antioxidant and antibacterial activities. Biomass Conv Bioref [Internet]. 2024 [cited 2024 Nov 25]; Available from: https://doi.org/10.1007/s13399-024-05804-x
42. Maulana I, Ginting B, Azizah K. Green synthesis of copper NPs employing Annona squamosa L extract as antimicrobial and anticancer agents. South African Journal of Chemical Engineering. 2023;46:65–71.
43. Islam MF, Islam S, Miah MAS, Huq AKO, Saha AK, Mou ZJ, et al. Green synthesis of zinc oxide nano particles using Allium cepa L. waste peel extracts and its antioxidant and antibacterial activities. Heliyon [Internet]. 2024 [cited 2024 Oct 17];10. Available from: https://www.cell.com/heliyon/abstract/S2405-8440(24)01461-0
44. kazemi S, Hosseingholian A, Gohari SD, Feirahi F, Moammeri F, Mesbahian G, et al. Recent advances in green synthesized NPs: from production to application. Materials Today Sustainability. 2023;24:100500.
45. Pushpanathan S, yahya S, Gunasekaran A, Natarajan SR, Kannan K, Krishnan K. Caffeic acid functionalized silver NPs: A bionanoformulation and its assessment of cell cycle and in vitro cytotoxicity. Next Nanotechnology. 2025;7:100105.
46. Bekele SG, Ganta DD, Endashaw M. Green synthesis and characterization of zinc oxide NPs using Monoon longifolium leave extract for biological applications. Discov Chem. 2024;1:5.
47. Chamkouri N, Jomehzadeh N, Naserzadeh N. Rapid biosynthesis and antibacterial activity of zinc oxide NPs using fruit peel of Punica granatumL as cellulose. Current Research in Green and Sustainable Chemistry. 2023;6:100366.
48. Samantaray A, Pradhan D, Behera B. Biosynthesized Silver NPs (AgNPs) from Trapa natans Peel Extract Exhibits Anti-Metastasis and Anti-Biofilm Potentials. IJPER. 2021;55:801–11.
49. Alyamani AA, Albukhaty S, Aloufi S, AlMalki FA, Al-Karagoly H, Sulaiman GM. Green Fabrication of Zinc Oxide NPs Using Phlomis Leaf Extract: Characterization and In Vitro Evaluation of Cytotoxicity and Antibacterial Properties. Molecules. 2021;26:6140.
50. Akbar N, Aslam Z, Siddiqui R, Shah MR, Khan NA. Zinc oxide NPs conjugated with clinically-approved medicines as potential antibacterial molecules. AMB Expr. 2021;11:104.
51. Abdelbaky AS, Abd El-Mageed TA, Babalghith AO, Selim S, Mohamed AMHA. Green Synthesis and Characterization of ZnO NPs Using Pelargonium odoratissimum (L.) Aqueous Leaf Extract and Their Antioxidant, Antibacterial and Anti-inflammatory Activities. Antioxidants (Basel). 2022;11:1444.
52. Ashraf H, Meer B, Iqbal J, Ali JS, Andleeb A, Butt H, et al. Comparative evaluation of chemically and green synthesized zinc oxide NPs: their in vitro antioxidant, antimicrobial, cytotoxic and anticancer potential towards HepG2 cell line. J Nanostruct Chem. 2023;13:243–61.
53. Lal S, Verma R, Chauhan A, Dhatwalia J, Guleria I, Ghotekar S, et al. Antioxidant, antimicrobial, and photocatalytic activity of green synthesized ZnO-NPs from Myrica esculenta fruits extract. Inorganic Chemistry Communications. 2022;141:109518.
54. Zafar M, Iqbal T. Green synthesis of silver and zinc oxide NPs for novel application to enhance shelf life of fruits. Biomass Conv Bioref. 2024;14:5611–26.
55. Saber MM, Mirtajani SB, Karimzadeh K. Green synthesis of silver NPs using Trapa natans extract and their anticancer activity against A431 human skin cancer cells. Journal of Drug Delivery Science and Technology. 2018;47:375–9.
56. Ifeanyichukwu UL, Fayemi OE, Ateba CN. Green Synthesis of Zinc Oxide NPs from Pomegranate (Punica granatum) Extracts and Characterization of Their Antibacterial Activity. Molecules. 2020;25:4521.

57. Loganathan S, Selvam K, Govindasamy M, Habila MA. Bioynthesis and characterization of zinc oxide NPs (ZnO-NPs) using Passiflora foetida Linn leaves extract and their biological applications. Biomass Conv Bioref [Internet]. 2024 [cited 2024 Oct 20]; Available from: https://doi.org/10.1007/s13399-024-05593-3
58. Saeed M, Al-Keridis LA, Khattak S, Alshuraym L, Alshammari N, Al-Amrah H, et al. Green Synthesis of Zinc Oxide NPs Using Egg White and Coriander Root Waste: Characterization and Anti-Cancer Efficacy in Hela Cells. Waste Biomass Valor. 2024;15:5639–55.
59. Bayat M, Zargar M, Astarkhanova T, Pakina E, Ladan S, Lyashko M, et al. Facile Biogenic Synthesis and Characterization of Seven Metal-Based NPs Conjugated with Phytochemical Bioactives Using Fragaria ananassa Leaf Extract. Molecules. 2021;26:3025.
60. Hameed H, Waheed A, Sharif MS, Saleem M, Afreen A, Tariq M, et al. Green Synthesis of Zinc Oxide (ZnO) NPs from Green Algae and Their Assessment in Various Biological Applications. Micromachines. 2023;14:928.
61. Iqbal J, Abbasi BA, Mahmood T, Kanwal S, Ahmad R, Ashraf M. Plant-extract mediated green approach for the synthesis of ZnONPs: Characterization and evaluation of cytotoxic, antimicrobial and antioxidant potentials. Journal of Molecular Structure. 2019;1189:315–27.
62. Yassin MT, Al-Otibi FO, Al-Askar AA, Elmaghrabi MM. Synergistic Anticandidal Effectiveness of Greenly Synthesized Zinc Oxide NPs with Antifungal Agents against Nosocomial Candidal Pathogens. Microorganisms. 2023;11:1957.
63. Ravichandran S, Radhakrishnan J, Sengodan P, Rajendran R, Ramalingam R, Arunachalam KD. Bio synthesis of Zinc oxide NPs using Clerodendrum phlomidis extract for antibacterial, anticancer, antioxidant and photocatalytic studies. J Mater Sci: Mater Electron. 2022;33:11455–66.
64. Shabbir Awan S, Taj Khan R, Mehmood A, Hafeez M, Rizwan Abass S, Nazir M, et al. Ailanthus altissima leaf extract mediated green production of zinc oxide (ZnO) NPs for antibacterial and antioxidant activity. Saudi Journal of Biological Sciences. 2023;30:103487.
65. Yang X, Cao X, Chen C, Liao L, Yuan S, Huang S. Green Synthesis of Zinc Oxide NPs Using Aqueous Extracts of Hibiscus cannabinus L.: Wastewater Purification and Antibacterial Activity. Separations. 2023;10:466.
66. Payani S, Bhaskar M, Kumar GS, Pradeepkiran JA. A study on antimicrobial and anticancer properties of Cissus quadrangulris using lung cancer cell line. Cancer Treatment and Research Communications. 2023;36:100732.
67. Hussain S, Liufang H, Shah SM, Ali F, Khan SA, Shah FA, et al. Cytotoxic effects of extracts and isolated compounds from Ifloga spicata (forssk.) sch. bip against HepG-2 cancer cell line: Supported by ADMET analysis and molecular docking. Front Pharmacol. 2022;13:986456.
68. Naiel B, Fawzy M, Halmy MWA, Mahmoud AED. Green synthesis of zinc oxide NPs using Sea Lavender (Limonium pruinosum L. Chaz.) extract: characterization, evaluation of anti-skin cancer, antimicrobial and antioxidant potentials. Sci Rep. 2022;12:20370.